HHS Public Access

Author manuscript

Neuron. Author manuscript; available in PMC 2021 February 19.

Published in final edited form as:

Neuron. 2020 February 19; 105(4): 742–758.e6. doi:10.1016/j.neuron.2019.11.012.

INTEGRATIVE AND NETWORK-SPECIFIC CONNECTIVITY OF THE BASAL GANGLIA AND THALAMUS DEFINED IN INDIVIDUALS

Deanna J. Greene[1,2,20,21], **Scott Marek**[3,20], **Evan M. Gordon**[4,5,6], **Joshua S. Siegel**[1], **Caterina Gratton**[7,8], **Timothy O. Laumann**[1], **Adrian W. Gilmore**[11], **Jeffrey J. Berg**[9], **Annie L. Nguyen**[3], **Donna Dierker**[2], **Andrew N. Van**[3], **Mario Ortega**[3], **Dillan J. Newbold**[3], **Jacqueline M. Hampton**[1], **Ashley N. Nielsen**[10], **Kathleen B. McDermott**[2,11], **Jarod L. Roland**[12], **Scott A. Norris**[3], **Steven M. Nelson**[4,5,6], **Abraham Z. Snyder**[2,3], **Bradley L. Schlaggar**[13,14,15], **Steven E. Petersen**[2,3,11,16,17], **Nico U.F. Dosenbach**[2,3,17,18,19]

[1]Dept. of Psychiatry, Washington University School of Medicine, St. Louis, MO

[2]Mallinckrodt Institute of Radiology, Washington University School of Medicine, St. Louis, MO

[3]Dept. of Neurology, Washington University School of Medicine, St. Louis, MO

[4]VISN17 Center of Excellence for Research on Returning War Veterans, Waco, TX

[5]Center for Vital Longevity, School of Behavioral and Brain Sciences, University of Texas at Dallas, Dallas, TX

[6]Dept. of Psychology and Neuroscience, Baylor University, Waco, TX

[7]Dept. of Psychology, Northwestern University, Evanston, IL

[8]Dept. of Neurology, Northwestern University, Evanston, IL

[9]Dept. of Psychology, New York University, New York, NY

[10]Institute for Innovations in Developmental Sciences, Northwestern University, Chicago, IL

[11]Dept. of Psychological and Brain Sciences, Washington University, St. Louis, MO

[12]Dept. of Neurological Surgery, University of California San Francisco, San Francisco, CA

[13]Kennedy Krieger Institute, Baltimore, MD

[14]Dept. of Neurology, Johns Hopkins University School of Medicine, Baltimore, MD

Correspondence: dgreene@wustl.edu (D.J.G.), smarek@wustl.edu (S.M.), dosenbachn@wustl.edu (N.U.F.D.).

AUTHOR CONTRIBUTIONS

Conceptualization: DJG, SM, EMG, JSS, JLR, SAN, NUFD; Methodology, Software, and Formal Analysis: DJG, SM, EMG, JSS, CG, TOL, DD, ANV, MO, DJN, AZS, BLS, SEP, NUFD; Investigation, Resources, and Data curation: DJG, MO, TOL, AWG, JJB, ALN, DJN, JMH, ANN, KBM, SMN, NUFD; Writing – Original Draft: DJG, SM, SAN, NUFD; Writing – Review & Editing: DJG, SM, EMG, JSS, CG, TOL, AWG, JJB, ALN, DD, ANV, MO, DJN, JMH, ANN, KBM, JLR, SAN, SMN, AZS, BLS, SEP, NUFD; Supervision: DJG, NUFD.

Declaration of Interests: The authors declare no competing interests.

[15]Dept. of Pediatrics, Johns Hopkins University School of Medicine, Baltimore, MD

[16]Dept. of Neuroscience, Washington University School of Medicine, St. Louis, MO

[17]Dept. of Biomedical Engineering, Washington University, St. Louis, MO

[18]Dept. of Pediatrics, Washington University School of Medicine, St. Louis, MO

[19]Program in Occupational Therapy, Washington University, St. Louis, MO

[20]These authors contributed equally

[21]Lead contact

SUMMARY

The basal ganglia, thalamus, and cerebral cortex form an interconnected network implicated in many neurological and psychiatric illnesses. A better understanding of cortico-subcortical circuits in individuals will aid in development of personalized treatments. Using Precision Functional Mapping – individual-specific analysis of highly sampled participants – we investigated individual-specific functional connectivity between subcortical structures and cortical functional networks. This approach revealed distinct subcortical zones of network-specificity and of multi-network integration. Integration zones were systematic, with convergence of cingulo-opercular control and somatomotor networks in the ventral intermediate thalamus (motor integration zones), dorsal attention and visual networks in the pulvinar, and default-mode and multiple control networks in the caudate nucleus. The motor integration zones were present in every individual, and correspond to consistently successful sites of deep brain stimulation (DBS; essential tremor). Individually variable subcortical zones correspond to DBS sites with less consistent treatment effects, highlighting the importance of PFM for neurosurgery, neurology, and psychiatry.

eToc

Individual functional mapping of the human subcortex revealed network integration zones (motor, cognitive, visual attention) that were variable and consistent across people. These individualized maps of cortico-subcortical circuits may have immediate clinical translation for invasive personalized treatments (e.g., deep brain stimulation).

Keywords

Basal ganglia; thalamus; subcortex; precision functional mapping; resting state; functional connectivity; deep brain stimulation; brain networks

INTRODUCTION

The thalamus and basal ganglia interconnect distant parts of the cerebral cortex via cortico-thalamo-cortical and cortico-striato-thalamic loops (Alexander et al., 1986). Hence, even small lesions in the thalamus or basal ganglia can be neurologically devastating, while similarly sized lesions in the cerebral cortex may go unnoticed (Bogousslavsky et al., 1988; Corbetta et al., 2015; Siegel et al., 2014). Because of their centrality, cortico-striato-thalamo-cortical loops also appear to underlie many neurological and psychiatric disorders, including

Parkinson disease, Tourette syndrome, and obsessive-compulsive disorder (Albin et al., 1989; Bradshaw and Sheppard, 2000; Mink, 2001). Thus, a better understanding of the functional organization of the thalamus and basal ganglia and their connectivity to the cortex is essential for understanding typical and atypical brain function.

Much of our current understanding of the anatomical connections and functional organization of the basal ganglia and thalamus originates from lesion, unit recording, and tracer studies in non-human primates (Alexander and Crutcher, 1990a; Haber, 2003; Selemon and Goldman-Rakic, 1985). This work originally suggested that parallel and segregated cortico-striato-thalamic circuits support different functional processes (e.g., motor, cognitive, limbic) (Alexander and Crutcher, 1990a, b; Alexander et al., 1986). This model has since been updated to account for findings demonstrating convergence of multiple spatially distant cortical projections to the subcortex, describing the circuits as “parallel and integrative” rather than purely parallel (Averbeck et al., 2014; Haber, 2003, 2016). Moreover, there is anatomical evidence from non-human primates that both cortical and cerebellar projections are integrated within the basal ganglia (Bostan and Strick, 2018). Thus, subcortical structures have been posited to contain sites/zones of integration of multiple functions, including executive control, reward processing, and spatial attention (Haber, 2016; Jarbo and Verstynen, 2015).

Neuroimaging studies have aimed to characterize human cortico-subcortical systems in light of the results from non-human primate studies. Much of this work has described segregated functional areas within subcortical structures based on functional and structural connectivity with the cerebral cortex, often defining each area by its preferential connectivity with a particular cortical region or network. These findings have been broadly consistent with the animal data, recapitulating sensorimotor, cognitive, and limbic subdivisions (Arsalidou et al., 2013; Barnes et al., 2010; Behrens et al., 2003; Choi et al., 2012; Di Martino et al., 2008; Fair et al., 2010; Greene et al., 2014; Lehericy et al., 2004; Zhang et al., 2008). Several studies have also supported the idea that subcortical subregions receive converging projections from multiple distinct cortical regions (Choi et al., 2017; Draganski et al., 2008; Hwang et al., 2017; Jarbo and Verstynen, 2015), which is consistent with the integrative model of cortico-subcortical circuitry (Haber, 2003).

The biggest caveat for all of the structural and functional connectivity studies of the basal ganglia and thalamus in humans, including our own, has been their reliance on group-averaged data. This approach was necessary because of the combination of small quantities of data per individual and the low signal-to-noise-ratio (SNR) of MRI. While group-average designs are valuable for understanding broad principles of subcortical functional organization, the specific organization of each individual is necessarily obscured. For example, the appearance of integration zones across functional networks in large samples may have been an artifact of individual variability rather than the true integration of signals from multiple networks. Since the basal ganglia and thalamus are relatively small structures, such features of functional organization specific to individuals are most prone to obfuscation by group averaging.

Individualized measures of integration and segregation of functional networks in the subcortex have the potential for significant clinical utility. For instance, subcortical structures are targeted using deep brain stimulation (DBS) for treatment of several neurological and psychiatric disorders, including essential tremor, Parkinson disease, dystonia, Tourette syndrome, obsessive-compulsive disorder, and treatment-resistant depression (Baizabal-Carvallo et al., 2014; Dandekar et al., 2018; Mink, 2009; Perlmutter and Mink, 2006; Skogseid, 2014; van Westen et al., 2015). Yet, specific target structures have variable success rates (McIntyre and Hahn, 2010; Wichmann and Delong, 2011). DBS of the ventral intermediate nucleus of the thalamus for treatment of essential tremor results in over 80% tremor reduction in all patients (Ondo et al., 1998; Perlmutter and Mink, 2006), while stimulation of the globus pallidus for treatment of dystonia results in only 30-50% symptom improvement across all patients and >75% improvement in only 33% of patients (Starr et al., 2006; Vidailhet et al., 2005). Thus, an individualized approach for characterizing the functional organization of the subcortex should shed new light on these variable response rates and potentially aid rapid clinical translation towards targeted individualized intervention.

A recent series of studies using Precision Functional Mapping (PFM: collecting large quantities of fMRI data in individuals) characterized the functional architecture of the cerebral cortex and cerebellum in individuals (Braga and Buckner, 2017; Filevich et al., 2017; Gordon et al., 2017b; Gordon et al., 2018; Gratton et al., 2018; Laumann et al., 2015; Marek et al., 2018; Poldrack et al., 2015). These studies have shown that the topographies of individual functional brain networks are reliable, externally valid, stable within an individual, and demonstrate individual-specific topological features of brain organization not evident in group-averaged data. Indeed, each individual differs systematically from the group average at particular cortical locations (Seitzman et al., 2019). If a similar degree of individual-specific functional network organization is present in the subcortex, accurately characterizing that organization could advance success rates of treatments like DBS.

The goal of the present study was to investigate the functional organization of the individual human basal ganglia and thalamus. Using the highly-sampled individuals from the Midnight Scan Club (MSC) dataset (Gordon et al., 2017b), we implemented a network-based functional connectivity approach to examine (1) functional network specificity and integration within the subcortex, and (2) individual variability and similarity of functional organization across subjects. This PFM approach aids in the advancement of our understanding of individual cortico-subcortical systems, and may be clinically relevant for more precise, patient-specific treatment of neurological and psychiatric disorders.

RESULTS

To measure cortico-subcortical resting state functional connectivity (RSFC) in ten highly-sampled individuals from the MSC dataset, blood oxygen level-dependent (BOLD) activity timecourses were extracted from each voxel in the basal ganglia and thalamus. Cortical timeseries were averaged across all vertices in each of nine canonical functional networks (Greene et al., 2014; Power et al., 2011), defined for each individual: visual, somatomotor hand, somatomotor face, cingulo-opercular, frontoparietal, dorsal attention, ventral attention,

salience, and default-mode (see STAR Methods). A subcortical voxel-to-cortical network connectivity matrix was generated for each subject by computing the Pearson correlation between the timecourses (concatenated across sessions) of each subcortical voxel and each cortical network. These connectivity matrices were used for all subsequent analyses. Given the small size of subcortical structures, additional highly-sampled, high-resolution BOLD data (2.6mm isotropic voxels) were collected from one of the individuals (MSC06) to validate results.

Our report focuses on two major properties of cortico-subcortical RSFC: (1) Network specificity (preferential connectivity with a single network) vs. Integration (strong connectivity with multiple networks) and (2) Group (common organization across individuals) vs. Individual (variable across individuals) (Fig. 1).

RSFC reliability requires larger amounts of data in subcortex than cortex

We addressed whether cortico-subcortical RSFC can be measured reliably in individuals using iterative split-half comparisons. Cortico-subcortical correlations were reliable for each individual in each subcortical structure of interest ($r > 0.6$ averaged across all voxels within each structure) with ~100 minutes of motion censored data per subject (Fig. S1A). More specifically, with >100 minutes of data, 87% of voxels in the caudate, 74% in the putamen, 54% in the globus pallidus, and 63% in the thalamus had high reliability ($r > 0.70$) (Fig. S1B). Low reliability in certain voxels was likely driven by the low temporal signal-to-noise ratio (tSNR) in these regions, as correlations between reliability and tSNR were significant for all subjects (mean $r = 0.20$, all p's $< .001$). These results indicate that more data are needed to achieve high reliability for cortico-subcortical RSFC than for cortico-cortical RSFC (45 minutes, as reported in Gordon et al., 2017b), and cortico-cerebellar RSFC (90 minutes, as reported in Marek et al. 2018), consistent with Noble et al., (2017).

Subcortical RSFC is measurable at the individual level

Fig. 2A displays group-averaged correlation maps within the subcortex for each cortical network, and Fig. 2B displays the correlations from two representative subjects; all subjects are shown in Fig. S2. To determine the robustness of the spatial patterns of these correlations, we compared the observed spatial patterns of correlations to those generated from a null distribution from rotated networks on the cortex. Spearman's rho between the actual correlations and percent stronger than null across all networks and subjects was 0.79 ± 0.07 (see STAR Methods for details).

Across subjects, there was similarity in subcortical RSFC for each network (Fig. 2C). The default-mode network was strongly functionally connected to the medial thalamus and large portions of the caudate extending into the ventral striatum. The visual and dorsal attention networks exhibited strong connectivity with the lateral and posterior regions of the thalamus corresponding to the location of the pulvinar and possibly the lateral geniculate nucleus. The frontoparietal and salience networks were functionally connected to the caudate (head, body). The ventral attention network was connected to the caudate, medial putamen, and medial thalamus, with stronger correlations in the left hemisphere. The cingulo-opercular network exhibited strong connectivity with a large portion of the ventral thalamus and

distinct anterior and posterior parts of putamen. Connectivity with the somatomotor networks was observed in the ventral and lateral portions of the thalamus, likely corresponding to ventral lateral and ventral posterior nuclei, with the somatomotor hand network peak correlations shifted posterior to that of the somatomotor face network (consistent with known somatotopy), although there was substantial overlap. In addition to these commonalities, variability across individuals was also evident (see Fig. S2). For example, Fig. 2B shows strong connectivity with the dorsal attention network in the caudate in MSC02, but not in MSC04.

The spatial pattern of correlations was compared to task fMRI responses elicited in the same individuals (Fig. 2D; Fig. S3). Task activations/deactivations validated the RSFC mapping of functional networks in the subcortex. Deactivations during a set of cognitive/perceptual tasks overlapped well with default-mode network connectivity in the head of the caudate and medial thalamus. Activations during these cognitive/perceptual tasks in the subcortex overlapped multiple control networks (e.g., cingulo-opercular, frontoparietal, ventral attention, dorsal attention, salience), sparing the default mode network (Fig. S4). In addition, activations in the subcortex in response to hand movements during a motor task (hand > foot contrast) overlapped well with positive correlations with the somatomotor hand network.

Individual-specific and group-level features of subcortical RSFC

Given that subcortical correlations show individual-specific features (Fig. 2B, S2) and consistency across subjects (Fig. 2C), we quantified the extent to which functional networks exhibited group vs. individual-specific features, using a similarity analysis as in Gratton et al. (2018) and Marek et al. (2018). For each subject, the RSFC data were randomly split in half, and the spatial similarity (Pearson r) of subcortical-cortical correlations with each network was calculated within each subject and between all subjects. To quantify variance in RSFC data shared across individuals (group effect) vs. variance unique to individuals (individual effect), we compared the within individual similarities (on-diagonal elements; individual effect) to the between individual similarities (off-diagonal elements; group effect), normalized by the sum of the group and individual effects. We conducted this analysis separately for the basal ganglia and thalamus, and demonstrated large group contributions (basal ganglia = 42% shared RSFC variance across subjects; thalamus = 39%) and individual contributions (basal ganglia = 58% RSFC variance specific to individuals; thalamus = 61%) (Fig. S5). Some control networks (frontoparietal, salience, dorsal attention, ventral attention) showed significantly less similarity across the group (i.e., more individual variability) than the somatomotor networks and the cingulo-opercular network ($\Delta z = -0.43$, $t = -25.15$, $p < 0.001$). Thus, the cingulo-opercular network stands in contrast to other control networks, demonstrating greater similarity to somatomotor networks in the subcortex.

Localization of functional integration zones in subcortex

Previous characterizations of basal ganglia and thalamic functional organization, using group-averaged data, often implemented a winner-take-all network approach (e.g., Choi et al., 2012; Greene et al., 2014; Zhang et al., 2008). This winner-take-all approach cannot account for integration of multiple networks within regions of the subcortex (Haber, 2016), since the functional maps are solely based on the network with the strongest connectivity. In

addition, a group-level approach to identifying functional integration could be spuriously affected by averaging across-subject variability. That is, the same anatomical location may exhibit connectivity to different networks in different individuals (Argall et al., 2006; Laumann et al., 2015; Van Essen, 2005), leading to the appearance of integration when those individual signals are averaged together. Therefore, we evaluated network co-localization at the individual-level in order to more accurately characterize the nature of functional integration within the subcortex.

We define integration as exhibiting strong functional connectivity with multiple networks. We implemented a modified winner-take-all analysis approach to account for zones of integration as well as zones that are “network-specific” (one network dominates). For every subcortical voxel, we identified the cortical network with the strongest correlation, as in a standard winner-take-all procedure. In accordance with Marek et al. (2018) we identified regions of integration vs. network-specificity by testing whether the RSFC with any other network was above a given threshold (66.7%) of the correlation with the winning network. We tested additional thresholds (50%, 75%), which yielded similar zones of integration (Fig. S6A). If the correlations with all the other networks were below this threshold for a given voxel, that voxel was considered “network-specific”. If the correlations with any of the other networks were within that threshold for a given voxel, that voxel was considered “integrative”, as multiple networks correlated strongly. An alternative approach based on effect size rather than percent differences yielded very similar results (Fig. S6B).

Fig. 3A and 3B display the subcortical network map for two representative subjects, and Fig. 3C shows the group average. All subjects are shown in Fig. S7. From the group average maps alone, one might suspect that the zones of integration could be artifactual due to subject averaging. However, we show that several integration zones were identified within all individuals, and thus, are not simply by-products of group averaging. One of the most notable integration zones was identified in the ventral intermediate thalamus, integrating the cingulo-opercular, somatomotor hand, and somatomotor face networks (Fig. 3D).

These functional network maps suggest that certain zones of integration and network-specificity appear similar across individuals. We quantified the overlap of integrative and network-specific voxels (irrespective of the specific network association) across subjects. Fig. 4 displays the overlap of (A) integrative voxels, demonstrating that certain zones were integrative in most subjects (e.g., ventral intermediate thalamus), and (B) network-specific voxels, demonstrating that certain zones were network-specific in most subjects (e.g., head of the caudate). In addition, certain integrative or network-specific zones represented the same networks across individuals, while others represented different networks across individuals. We further explore this individual similarity and variability in network associations below.

In order to benchmark the degree of integration in the basal ganglia and thalamus compared to the cerebellum and cerebral cortex, we computed the percent of voxels/vertices within each brain structure that were integrative, as defined by the 66.7% threshold used in the analyses above. This computation demonstrated that a greater percentage of the subcortex (45%) was integrative compared to the cerebellum (35%) and cerebral cortex (31%). Within

the subcortex, we found that the thalamus was 45% integrative, the globus pallidus was 52% integrative, the putamen was 42% integrative, and the caudate was 37% integrative. Note that the thalamus was more integrative than the caudate, even though the thalamus is 240% larger in size. Therefore, the increased integration in the subcortex is not likely caused by the smaller size of the structures.

To ensure that integration was not driven by methodological factors, we tested different numbers of *a priori* cortical networks (i.e., 7 and 15 networks derived from Infomap) as well as the effect of proximity to multiple networks (i.e., voxels with a greater number of distinct networks surrounding it would be disproportionately biased to be defined as integrative). We found that subcortical integrative voxels were not substantially altered by differences in the number of *a priori* cortical networks (Fig. S8). The percent of integrative voxels (45% reported above) was 40% when using the 7-network Infomap solution and 48% when using the 15-network Infomap solution. Community density analyses support the idea that integration was not driven by proximity to more networks, as an average of 46% of voxels with a community density > 1 were defined as integrative (range 35-57% across subjects). Thus, high community density did not bias whether a voxel was defined as integrative or network-specific.

Further, the higher-resolution (2.6 mm) data collected for MSC06 confirmed the presence of integrative voxels in the subcortex, suggesting that integration was not a simple byproduct of mixing signals within 4 mm voxels. Rather, we found a slightly higher percent of subcortical integrative voxels in MSC06 with the higher-resolution data (51% vs. 45%) that was largely due to more integrative voxels in the thalamus (62% with 2.6mm vs. 38% with 4mm). Thus, integration in the thalamus was not related to the resolution of the data.

Three clusters of network integration are present in the subcortex

To determine which networks preferentially integrate with each other, we quantified the number of integrative subcortical voxels for each network-network pair (e.g., number of voxels integrating frontoparietal and salience networks) summed across subjects. We normalized these summed values by the total number of integrative voxels, resulting in a percentage of integrative voxels for each network-network pair. This network-by-network matrix was submitted to hierarchical clustering, and revealed three clusters of network integration, indicating preferential integration of particular networks (Fig. 5A; cophenetic r = 0.82).

We found a “motor integration” cluster, which demonstrated integration of the somatomotor hand, somatomotor face, and cingulo-opercular networks. Topographically, this integration was most prominent in the ventral intermediate thalamus (Fig. 5B). We also found a “cognitive integration” cluster, which demonstrated preferential integration of the ventral attention, frontoparietal, salience, and default-mode networks. Integration of these higher-order networks was most prominent in the caudate (Fig. 5B). A third “visual attention integration” cluster included the dorsal attention and visual networks. Integration of these networks was most prominent in the posterior portion of the thalamus (corresponding to the pulvinar; Fig. 5B). These three clusters were identified at the individual subject level in both

the 4 mm (Fig. 5C) and 2.6 mm (Fig. 5D) resolution data. This three cluster solution was replicated using modularity, a graph theoretic clustering algorithm (Newman, 2006).

The basal ganglia and thalamus contain four distinct types of functional zones

Given our framework for understanding cortico-subcortical RSFC (Fig. 1), we investigated which basal ganglia and thalamus voxels exhibited properties of integration vs. network-specificity, as well as whether the network(s) functionally connected with these voxels were consistent or variable across individuals. Voxels were considered network-specific if they exhibited strong RSFC to one network only, and were considered integrative if they exhibited strong RSFC to more than one network. Voxels were then considered consistent across the group if more than five subjects shared the same network assignment(s); otherwise, they were considered individually-specific. These criteria delineated four types of functional zones in the subcortex: (1) Group Network-Specific zones with consistent network-specificity in most subjects; (2) Group Integrative zones with integration of the same networks in most subjects; (3) Individual Network-Specific zones with variable network-specificity across subjects; and (4) Individual Integrative zones with variable network integration across subjects. To assess confidence in these zone assignments, we implemented a jack-knifing procedure in which the functional zones were assigned as just described ten times, leaving out a unique subject with each iteration. The percent of iterations a given voxel was assigned to a functional zone provides a confidence level for the functional zone assignment, and is illustrated in Fig. 6A. Variability in signal intensity after nonlinear atlas registration was not related to whether a voxel was identified as Group or Individual (comparison of signal intensity for Group vs. Individual voxels: $t = 0.65$, $p = 0.52$), suggesting that the network assignment was not significantly related to anatomical alignment.

Fig. 6B displays the RSFC profiles of example seed regions in the basal ganglia and thalamus from representative MSC subjects (varies by panel) that exemplify each of the four zones. Group Network-Specific zones included regions in the medial thalamus with preferential RSFC to the default-mode network in most subjects, and regions in the head of the caudate with preferential RSFC to the salience network in most subjects. Group Integrative zones were primarily located in the ventral intermediate thalamus with integration of cingulo-opercular and somatomotor networks (hand and face) in all ten subjects, and in the caudate with integration of control networks. Individual Network-Specific zones included the head of the caudate with preferential RSFC to the frontoparietal, ventral attention, salience, or default-mode networks. These zones were also found in regions of the putamen and dorsal thalamus with preferential RSFC to the cingulo-opercular, dorsal attention, salience, or somatomotor hand networks. Individual Integrative zones were located in portions of the putamen and in the ventral thalamus with variable integration of the default-mode, frontoparietal, ventral attention, salience, cingulo-opercular, and somatomotor networks.

DISCUSSION

We characterized the functional network organization of the human basal ganglia and thalamus at the level of the individual, using Precision Functional Mapping (PFM) with highly-sampled individual-subject fMRI data from the Midnight Scan Club (MSC) dataset. Our analyses revealed distinct zones of network integration (strong functional connectivity with multiple networks) in 45% of the subcortex and network-specificity (strong functional connectivity with a single network) in 55% of the subcortex. We also found individual variability in cortico-subcortical RSFC in 43% of the subcortex and commonalities across the group in 57% of the subcortex. Integration zones were found in reliably localizable regions, such that the ventral intermediate thalamus integrated cingulo-opercular and somatomotor networks (motor integration zones), the pulvinar integrated dorsal attention and visual networks (visual attention integration zones), and the caudate nucleus integrated default-mode and several executive control networks (cognitive integration zones). The motor integration zones were remarkably consistent across all ten individuals, suggesting a vital role for the cingulo-opercular network in top-down control of motor functions. Integration zones were also found in regions of the putamen and pallidum, with individually variable integration of control and somatomotor networks. Overall, the ability to reliably measure cortico-subcortical RSFC in individuals using PFM holds promise for clinical treatments that require precise targeting of subcortical structures, such as deep brain stimulation (DBS).

Individual specificity and consistency in subcortical RSFC varies by network

We found individual variability in subcortical RSFC that was not captured by the group average and could only be elucidated by individual-level analyses, in addition to broad similarities across subjects that were captured by the group average. The existence of both individual specific and shared features is consistent with recent cortical and cerebellar RSFC findings (Gratton et al., 2018; Marek et al., 2018). Given the phylogenetically older origin of the subcortex compared to the cortex (Grillner et al., 2013) and the small size of subcortical structures, one might have expected less individual variability in the subcortex; yet we found strong individual-level contributions.

Interestingly, particular functional networks in the subcortex – salience, frontoparietal, ventral attention, and dorsal attention – were relatively more variable across individuals, while others – cingulo-opercular and somatomotor – were more consistent. Recent studies have suggested that in the cortex, networks supporting top-down control show greater individual differences than other networks (Finn et al., 2015; Gratton et al., 2018; Horien et al., 2019; Laumann et al., 2015; Miranda-Dominguez et al., 2014; Mueller et al., 2013). It is notable that the cingulo-opercular network, an executive control network (Crittenden et al., 2016; Dosenbach, 2008; Duncan and Owen, 2000; Nelson et al., 2010; Neta et al., 2015; Sadaghiani and D'Esposito, 2015), was relatively more stable across individuals in the subcortex. Thus, it stands as an intriguing exception to the more individually variable control networks (see below for further discussion). Further investigation using larger cohorts of highly-sampled individual-specific datasets will help elucidate how these differences in individual variability across networks relate to individual differences in behavior.

PFM differentiates four types of subcortical functional zones

Our individual-specific approach identified four types of functional zones within subcortical structures: Group Network-specific, Group Integrative, Individual Network-specific, and Individual Integrative. Distinguishing these functional zones is possible only by obtaining individual-level results. Functional parcellation of subcortical structures in individuals has been conducted with conventional quantities of resting state fMRI data (5-20 min per subject) (Garcia-Garcia et al., 2017; Janssen et al., 2015). However, the methods employed in these studies relied upon a group-average reference and clustering algorithms within small structures, which are susceptible to bias due to spatial autocorrelation. Further, we show that 100 minutes or more are needed to reliably estimate individual cortico-subcortical RSFC in some structures (globus pallidus, thalamus). Thus, with the high reliability afforded by PFM, we were able to identify functional zones beyond broad subdivisions of the subcortex in individuals. Indeed, more data were required to obtain reliable estimates in the subcortex compared to the cortex, which may be due to biological differences between structures that affect BOLD signal properties, or due to methodological differences, such as distance from the MR head coil, susceptibility artifact, and/or reduced gray-white contrast.

The subcortex contains sites of functional network integration and specificity

We provide compelling human *in vivo* evidence for the existence of network-specific and integrative zones in subcortical structures, consistent with animal models of “parallel and integrative” cortico-subcortical circuits (Averbeck et al., 2014; Haber, 2003, 2016). The presence of both network-specific and integrative functional zones in the subcortex may be critical for coordinating behavior that requires interactions between functions subserved by distinct functional networks, depending on the demands of the environment (Haber, 2003). That is, certain behavioral contexts may require independent functioning of a specific network, while others may require behavior that involves coordination of multiple network functions.

Previous human neuroimaging studies that discussed convergence zones or hubs within the basal ganglia and thalamus did not consider the functional network organization of the brain and/or necessarily relied upon group averaging (Choi et al., 2017; Draganski et al., 2008; Hwang et al., 2017; Jarbo and Verstynen, 2015), both of which could lead to the appearance of integration artifactually. For example, apparent integration of anatomically-defined frontal and parietal regions may simply reflect the anatomically distributed organization of the frontoparietal network rather than integration of multiple networks. In addition, group averaging may create the spurious appearance of integration since brain organization is spatially variable, and thus, the same brain stereotactic location may be linked to different networks in different individuals (Argall et al., 2006; Laumann et al., 2015; Van Essen, 2005). If a particular location is connected to different networks in different individuals, averaging those signals across the group can result in a signal correlated with multiple networks, even if this “integration” is not present in individual subjects. Consequently, mapping zones of integration must be done at the level of the individual.

Our results are in line with existing evidence from structural (Draganski et al., 2008; Jarbo and Verstynen, 2015) and functional connectivity studies (Garrett et al., 2018; Hwang et al.,

2017) that suggest the basal ganglia and thalamus play central roles in the functional integration of cortical networks. One way in which this integration may occur is via cortico-striato-thalamo-cortical loops. Specifically, cortical inputs are integrated within the basal ganglia and thalamus before being projected diffusely to multiple cortical networks (Alexander et al., 1986; Averbeck et al., 2014; Draganski et al., 2008; Jarbo and Verstynen, 2015; Jones, 1998; Metzger et al., 2013). Thus, the basal ganglia and thalamus simultaneously receive and integrate signals from the cortex and transmit signals to multiple cortical functional networks (Bosch-Bouju et al., 2013; Jones, 1998). Our results provide corroborating evidence that specific focal regions of subcortex are functionally connected to multiple cortical networks.

From fMRI data, we cannot determine whether functional integration in the subcortex reflects direct convergence of projections to and from multiple cortical networks or interdigitated projections at the neuronal level. Animal research suggests that overlap of terminal fields reflects interdigitated projections (Selemon and Goldman-Rakic, 1985), but further investigation is needed. Our results can inform future animal work by guiding particular anatomical targets of study. For example, integration zones that are common across subjects – e.g., motor integration zones in the thalamus – may be particularly good candidates for investigating projections at the neuronal level. Though the definition of integration zones could be influenced by our methods, we showed consistent results across multiple approaches for defining integrative voxels (Fig. S6). Further, we corroborated these integration zones with higher resolution (2.6 mm) data (Fig. 5), which showed even greater integration in the thalamus than with 4 mm data.

In addition, it is important to note that the cortico-subcortical RSFC analyses presented here did not account for connectivity within the subcortex (e.g., thalamo-striatal connections). Future methods that can account for both subcortico-subcortical and cortico-subcortical connections may provide further insight into functional network integration within the subcortex.

Functional networks converge preferentially in focal regions of the subcortex

With the precision afforded by PFM, we were able to delineate specific regions within subcortical structures that integrated multiple networks. These integration zones were found with standard (4mm) as well as high-resolution (2.6mm) fMRI data. They may serve as critical hubs connecting cortical functional networks via cortico-striato-thalamo-cortical loops. Most studies investigating functional network hubs, including our own, have largely ignored or de-emphasized subcortical structures (e.g., He and Evans, 2010; Power et al., 2011; Power et al., 2013; Yeo et al., 2011). Yet, it is possible that hubs critical for information flow between cortical networks are located in the subcortex. The integration zones described here reflect the precise location of putative subcortical hubs and the specific functional networks that converge within them.

Motor integration zones—The integration zones that were consistently present in all ten individuals combined the somatomotor hand, somatomotor face, and cingulo-opercular networks in the ventral intermediate portion of the thalamus. Thalamic integration of these

networks suggests that the cingulo-opercular network might exert some level of control over motor outputs via the thalamus. The current dominantly held view is that the cingulo-opercular network is involved in sustained aspects of task control (Crittenden et al., 2016; Dosenbach et al., 2008; Dosenbach et al., 2007; Dosenbach et al., 2006; Duncan and Owen, 2000; Sadaghiani and D'Esposito, 2015). The cingulo-opercular network has properties similar to other controls networks (e.g., frontoparietal, salience), such as cue activations and error monitoring (Dosenbach et al., 2007; Neta et al., 2015; Petersen and Posner, 2012), that are distinct from lower-level processing networks (e.g., somatomotor networks). However, there is some evidence that a subset of cingulo-opercular regions in the cortex, unlike other control networks, link to somatomotor networks (Gordon et al., 2018; Power et al., 2011), and show activity corresponding to the moment a response is made (Gratton et al., 2017). Non-human primate studies have identified “cingulate motor areas” that play a role in motor planning, preparation, and execution (Dum and Strick, 1993). Further, data from stroke patients suggest that some cingulo-opercular regions are necessary for executing motor functions (Rinne et al., 2018). Interestingly, functional connectivity between the cingulo-opercular and somatomotor networks increases with development in a manner that suggests maturation of inhibitory control (Marek et al., 2015). Thus, the cingulo-opercular network appears to be linked to somatomotor networks in a way that is distinct from other control networks. Our results indicate that the ventral intermediate region of the thalamus may be a critical locus of this integration.

Visual attention integration zones—In the posterior thalamus, corresponding to the location of the pulvinar, we observed preferential integration of the dorsal attention and visual networks. Previous work in non-human primates has shown that the pulvinar is involved in attentional selection and regulating the transmission of information across visual cortex (Petersen et al., 1985; Petersen et al., 1987; Saalmann et al., 2012). Human fMRI data also support a role for the pulvinar in attentional filtering of irrelevant information (Fischer and Whitney, 2012). Here, we show that the pulvinar is a site of integration of the visual network, which comprises primary and association visual areas, and the dorsal attention network, which comprises posterior parietal cortex and frontal eye fields and is involved in spatial attention (Corbetta and Shulman, 2002). Diffusion imaging in humans and anatomical tracing studies in nonhuman primates support this notion of integration. Specifically, structural connections exist between the pulvinar and primary and association visual cortex. Projections from the frontal eye fields and intraparietal sulcus indirectly innervate the pulvinar via ascending projections from the superior colliculus, forming cortico-colliculo-pulvino-cortical loops (Leh et al., 2008; Shipp, 2001, 2004; Weller et al., 2002). These structurally and functionally integrative connections of the pulvinar suggest it may operate by coordinating attentional functions via integration of the visual and dorsal attention networks (Kastner and Pinsk, 2004; Shipp, 2004).

Cognitive integration zones—Particular networks supporting top-down control and attention (fronto-parietal, salience, ventral attention) and the default-mode network showed preferential integration in certain regions of the subcortex. Integration zones in the caudate and dorsal thalamus exhibited similar convergence of networks across individuals, while integration zones in the putamen and pallidum exhibited individually variable convergence

of these networks. The zones in the caudate overlap substantially with non-human primate studies showing converging projections from widespread areas of the frontal lobe, including the ventromedial prefrontal cortex (PFC), anterior cingulate cortex, ventrolateral PFC, and dorsal PFC (Averbeck et al., 2014). These regions are part of the default mode (ventromedial PFC), salience (anterior cingulate cortex), ventral attention (ventrolateral PFC), and frontoparietal (dorsal PFC) networks. Similarly, in the dorsal thalamus, non-invasive diffusion studies in humans show structural connectivity to widespread areas of PFC (Behrens et al., 2003). Together, our results suggest that these regions may act to functionally integrate control and default mode networks similarly across individuals in the caudate and dorsal thalamus, but variably across individuals in the putamen and pallidum.

Clinical importance of subcortical functional integration zones

Given the involvement of cortico-subcortical circuits in many neurological and psychiatric disorders (Albin et al., 1989; Bradshaw and Sheppard, 2000; Drysdale et al., 2017; Greene et al., 2017; Liston et al., 2011; Mink, 2003), the functional integration zones we uncovered may be hotspots for neurological and psychiatric morbidity. Zones with common profiles across individuals may be affected similarly across disorders, while zones with variable profiles across individuals may be important for understanding heterogeneity across and within specific disorders. It is also possible that integration zones may be more affected in psychopathology than network-specific zones, relating to the complex nature of many neuropsychiatric disorders. One might expect that the impairments often seen across multiple functional domains (motor, cognitive, affective) in many disorders (Heller, 2016; Luking et al., 2016; Ring and Serra-Mestres, 2002) are more likely the result of alterations to integration zones, whereas alterations to network-specific zones may only affect one or a few functions. Thus, our results can guide future targets of study, both in understanding the functional role of these zones as well as in understanding how each may be affected (and potentially targeted for treatment) in psychopathology.

Precision functional mapping of subcortical structures may guide targets for deep brain stimulation (DBS)

PFM has the potential to improve success of interventions that target subcortical structures, most notably DBS. Presently, it is unclear why certain DBS target sites have more consistent efficacy than others, and how stimulation of a given target modulates functional networks to alter behavior and/or clinical outcomes (Alhourani et al., 2015). There is work, primarily in Parkinson disease (PD), investigating the relationship between anatomical locations of stimulation and clinical outcome (reviewed in Horn, 2019). In particular, two recent studies (Bot et al., 2018; Horn et al., 2019) pinpointed a specific subthalamic nucleus location as the best predictor of treatment response in PD. Though promising, this anatomically-defined location still only explains 27% of the variance in clinical outcome. Further, there is a high degree of overlap between stereotactic coordinates of responders and non-responders. Thus, better accounts of function and individual neuroanatomical variability may improve efficacy of DBS and other treatment approaches, such as focused ultrasound (Bot et al., 2018; Horn, 2019; Horn et al., 2019; Nestor et al., 2014; Zaaroor et al., 2018). It has been shown, using typical amounts of functional connectivity data per subject (6-12 min), that stimulation sites previously reported to be effective for the same disease belong to the same functional brain

networks (e.g., DBS of the globus pallidus and transcranial magnetic stimulation of primary motor cortex in PD), highlighting the promise of network-based approaches (Fox et al., 2014). However, these studies did not account for the possibility that individual variability in subcortical organization may influence the consistency of DBS success.

Our results present the compelling possibility that PFM could explain clinical variability of DBS outcomes and help guide DBS placement in the future (Fig. 7). We speculate that PFM could ultimately be used to locate patient-specific nodes of a particular functional network for which stimulation improves symptoms. For example, the DBS sites most commonly targeted for essential tremor fall in the Group (i.e., low variability) motor integration zones in the thalamus identified in the present study; DBS sites commonly targeted for PD and dystonia fall in Individual-specific (i.e., highly variable) sites in the globus pallidus internal (GPi). Thus, the consistent clinical improvement following stimulation of the ventral intermediate thalamic DBS target (i.e., >80% improvement in all essential tremor patients) (Perlmutter and Mink, 2006) may reflect the highly consistent location of the motor integration zones across individuals. By contrast, the GPi location targeted for PD and dystonia varies in its functional connectivity across subjects. This finding may account for increased variability in clinical outcomes (Campbell et al., 2012; Campbell et al., 2008; Hershey et al., 2010; Houeto et al., 2003; Mandat et al., 2006; Perriol et al., 2006; Starr et al., 2006; Wodarg et al., 2012) and lack of ability to identify optimal stimulation regions within the GPi target in group-level studies of DBS outcomes (Nestor et al., 2014; Tolleson et al., 2015). Perhaps there is a relationship between clinical response rate to GPi DBS and a particular functional connectivity pattern at the stimulation site. If DBS in PD and dystonia were able to consistently target the same functional network(s), clinical outcomes might improve considerably. Examining the relationships between the target functional zones identified in the present study and clinical DBS outcomes is an exciting avenue of future research with the potential to inform clinical care.

STAR METHODS

Contact for Reagent and Resource Sharing

Further information and requests for resources should be directed to and will be fulfilled by the Lead Contact, Deanna Greene (dgreene@wustl.edu)

Experimental Model and Subject Details

Data from ten young adults (24-34 years old; 5 females; all right handed) from the publicly available Midnight Scan Club (MSC) dataset were used in the present study (https://openfmri.org/dataset/ds000224/). Details about the dataset and processing have been previously described (Gordon et al., 2017b). Here, we describe information about the data and processing that is relevant to the current project, and the specific analyses employed.

Participants and Study Design—The MSC dataset includes structural and functional MRI data, as well as behavioral measures from 10 individuals (5 females, ages 24-34). fMRI data were collected over 10 sessions, each occurring on a separate day, beginning at midnight. Daily sessions were conducted in close succession, with all sessions completed

within 7 weeks for all participants. All participants provided written informed consent. Procedures were approved by the Washington University Institutional Review Board and School of Medicine Human Studies Committee. During each scanning session, participants completed a 30 min resting-state run followed by fMRI scans during four other tasks: a motor task, a semantic task, a coherence task, and an incidental encoding memory task. MRI acquisition parameters and tasks are described below.

METHOD DETAILS

MRI image acquisition—Participants underwent 12 imaging sessions on a Siemens TRIO 3T MRI scanner, beginning at midnight, over the course of 3-6 weeks each. The first two sessions consisted of structural MRI scans and the following ten sessions consisted of functional MRI (fMRI) scans. Structural images included four T1-weighted scans (TE=3.74ms, TR =2400ms, TI = 1000ms, flip angle=8°, 0.8mm isotropic voxels, 224 sagittal slices), four T2-weighted images (TE=479ms, TR=3200ms, 0.8mm isotropic voxels, 224 sagittal, 224), four MRA and eight MRV scans (not used in the present study; see Gordon et al., 2017b for details). Functional images included 300min total of eyes-open resting-state fMRI BOLD data (30min per session) and 350min total of task fMRI BOLD data (see below) using a gradient-echo EPI BOLD sequence (TE=27ms, TR=2.2s, flip angle=90°, 4mm isotropic voxels, 36 axial slices). Gradient echo field map images (one per session) were acquired with the same parameters.

One participant (MSC06) underwent an additional 12 imaging sessions on a Siemens Prisma 3T MRI scanner, consisting of fMRI scans with higher resolution (gradient-echo EPI BOLD sequence: multiband factor 4, TE=33ms, TR=1.1s, flip angle=84°, 2.6mm isotropic voxels, 56 axial slices).

QUANTIFICATION AND STATISTICAL ANALYSIS

MRI Data Processing and Surface Registration—MRI data were preprocessed and sampled to the cortical surface as previously described in detail (Marek et al., 2018). The processing code is code is publicly available at https://github.com/MidnightScanClub. Here, we briefly describe the steps.

Structural MRI: Cortical surfaces were generated using procedures as in (Laumann et al., 2015). Briefly, using FreeSurfer v5.3, each subject's averaged T1-weighted image was run through the recon-all processing pipeline to generate the anatomical surface (Dale et al., 1999; Fischl et al., 1999). This surface was manually edited using Freeview to maximize accuracy, and registered into fs_LR_32k surface space using a flexible Multi-modal Surface Matching algorithm (Glasser et al., 2016; Van Essen et al., 2012). The subject-specific surfaces in native space were transformed into Talairach volumetric space by applying an average T1-to-Talairach transform.

Functional MRI preprocessing: All functional data were preprocessed in volume space to reduce artifact and maximize cross-session registration, including (i) slice timing correction, (ii) intensity normalization to a whole brain mode value (across voxels and TRs) of 1000 for each run, and (iii) within-run correction for head motion. Then, the functional data were

registered to Talairach atlas space using the average T2-weighted image and the average T1-weighted image. Distortion correction was applied using a mean field map for each subject and applying that field map to each fMRI session, as previously described (Gordon et al., 2017b). Registration, atlas transformation, distortion correction, and resampling to 3 mm isotropic atlas space were combined into a single interpolation using FSL's applywarp tool (Smith et al., 2004). To account for anatomical differences between subjects, we non-linearly warped each subject's atlas-aligned T1 to MNI space using FSL's FNIRT. Volumetric time series subsequently were registered to each subject's registered T1. All between subjects analyses and group average analyses were carried out on these atlas-transformed volumetric time series.

Functional connectivity preprocessing: Additional preprocessing steps were applied to the resting-state fMRI data to reduce spurious variance unlikely to reflect neuronal activity. First, a motion censoring procedure as described in (Power et al., 2014) was implemented, which in combination with our other processing steps has been shown to best account for motion artifact (Ciric et al., 2017). Temporal masks were created to flag motion-contaminated volumes based on framewise displacement (FD) and the temporal derivative of the root mean squared variance over voxels (DVARS). Frames with FD > 0.2mm or DVARS > 5.36 were flagged. Two subjects (MSC03, MSC10) required additional correction for artifactual high-frequency motion in the phase encoding direction (anterior-posterior) as previously described (Gordon et al., 2017b; Gratton et al., 2018). Application of the temporal masks resulted in retention of 5704 ± 1548 volumes per subject (range 2691-7530) (for more details, see Gordon et al., 2017b). Thus, even the subject with the most motion-contaminated data retained nearly 100 min. Then, the data underwent additional processing steps, including (i) demeaning and detrending, (ii) interpolation across censored volumes using least-squares spectral estimation of the values at the censored timepoints, (iii) temporal band-pass filtering (0.005 Hz < f < 0.01 Hz), and (iv) multiple regression of nuisance variables, including the global signal, principle components of ventricular and white matter signals (see below "Component-based nuisance regression"), and motion estimates derived by Volterra expansion (Friston et al., 1996), applied in a single step to the filtered, interpolated BOLD time series. Finally, censored volumes were removed from the data for all subsequent analyses.

For the additional 2.6mm resolution data collected from MSC06, the data were processed the same as the 4mm resolution data, with the following exceptions: (1) FD measurements were corrected for artifactual high-frequency motion in the phase encoding direction, (2) the FD threshold for motion censoring was 0.1mm, and (3) the DVARS threshold for motion censoring was 6.

The cortical data were then registered to the surface (see above, *Structural MRI*). The cortical surface data and volumetric subcortical and cerebellar data were combined into CIFTI data format using Connectome Workbench (Marcus et al., 2011). Voxels in the cerebellum and subcortex (including thalamus, caudate, putamen, pallidum, nucleus accumbens, amygdala, and hippocampus) were derived from the FreeSurfer segmentation of each subject's native average T1 image, transformed into Talairach atlas space. Finally, the cortical surface functional data were smoothed (2D geodesic, Gaussian kernel, σ = 2.55mm).

Due to the relatively small size of the basal ganglia and thalamus, we did not perform spatial smoothing within the volume and we up-sampled the fully processed data to 2mm isotropic voxels. To mitigate effects of signal contamination from nearby cortical areas (e.g., insula signal adjacent to the putamen), we regressed the time course of BOLD activity from any cortical vertices within 20mm of a subcortical voxel, similar to strategies taken in previous work on subcortical functional connectivity (Choi et al., 2012; Greene et al., 2014).

Component-based nuisance regression: The filtered BOLD time series underwent a component-based nuisance regression approach as in Marek et al. (2018) and Raut et al. (2019), incorporating elements of previously published methods (Behzadi et al., 2007). Nuisance regressors were extracted from individualized white matter and ventricle masks, first segmented by FreeSurfer (Fischl, 2012), then spatially resampled in register with the fMRI data. Since voxels surrounding the edge of the brain are particularly susceptible to motion artifacts and CSF pulsations (Satterthwaite et al., 2013; Yan et al., 2013), a third nuisance mask was created for the extra-axial compartment (edge voxels; Patriat et al., 2015) by thresholding the temporal standard deviation image (SDt > 2.5%) (Behzadi et al., 2007), excluding a dilated whole brain mask. Voxel-wise nuisance time series were dimensionality reduced as in CompCor (Behzadi et al., 2007), except that the number of retained regressors, rather than being a fixed quantity, was determined, for each noise compartment, by orthogonalization of the covariance matrix and retaining components ordered by decreasing eigenvalue up to a condition number of 30 ($\lambda_{max}/\lambda_{min} > 30$). The retained components across all compartments formed the columns of a design matrix, X, along with the global signal, its first derivative, and the six time series derived by retrospective motion correction. The columns of X are likely to exhibit substantial co-linearity. Therefore, to prevent numerical instability owing to rank-deficiency during nuisance regression, a second-level SVD was applied to XX^T to impose an upper limit of 250 on the condition number. This final set of regressors was applied in a single step to the filtered, interpolated BOLD time series.

Analysis Overview

Cortico-subcortical FC: To capture cortico-subcortical resting state functional connectivity (RSFC), we measured RSFC between subcortical voxels and cortical functional networks. First, we identified each subject's individual cortical functional network organization using the graph-theory-based Infomap algorithm for community detection (Rosvall and Bergstrom, 2008), following Power et al. (2011). Derivation of the Infomap communities (representing networks) for each subject has been previously described in Gordon et al. (2017b) and Marek et al. (2018). Briefly, Pearson r correlations were computed between the BOLD time series (concatenated across sessions) among all cortical vertices, generating a 59,412 vertex x 59,412 vertex correlation matrix. The matrix was thresholded across a range of densities from 0.1% to 5%, and community assignments were generated from the Infomap algorithm for each threshold. To assign putative network identities to each subject's communities, a matching procedure to networks identified for an independent group of 120 subjects was used (see Gordon et al., 2017b; Marek et al., 2018 for details). Figure 8A shows these cortical functional network assignments for each individual subject and for the group average.

For the purposes of our subcortical-cortical analyses, we selected nine cortical functional networks (the same 9 for all subjects) that have been previously well-characterized in the cortex by multiple investigators using varying methods (e.g., Damoiseaux et al., 2006; Gordon et al., 2016; Power et al., 2011; Yeo et al., 2011) and have been examined with respect to RSFC with the subcortex (Greene et al., 2014): somatomotor hand, somatomotor face, visual, frontoparietal, cingulo-opercular, dorsal attention, ventral attention, salience, and default-mode. These cortical networks are shown for each subject in Fig. 8A. Then, we computed the average time series across vertices for each of these nine cortical networks in each hemisphere separately, and correlated them with the time series from each subcortical voxel (voxels within each subject's thalamus, caudate, putamen, pallidum, and nucleus accumbens; Figure 8B) in the ipsilateral hemisphere (consistent with anatomical connections). Note that our results do not appreciably change when the analyses are conducted using correlations from both hemispheres (83% of subcortical voxels have identical "winning" network assignments). Given the close anatomical proximity of several subcortical structures to certain regions of cortex, we regressed the cortical signal within 20mm of the subcortex from each subcortical voxel time series in order to mitigate potential artifactual inflations in correlations due to signal bleed, similar to previous subcortical-cortical FC studies (Choi et al., 2012; Greene et al., 2014). The resulting subcortical voxel-to-cortical network correlation matrices (one per subject) were used for subsequent analyses.

The same procedures were applied to the whole group of subjects in order to compute the group averaged subcortical voxel-to-cortical network correlation matrix. The nine cortical functional networks were selected from the group average Infomap communities as reported in Marek et al. (2018).

We repeated these procedures after partialing out the time series of activity of each cortical network from every other network (as in Greene et al., 2014) before quantifying RSFC between each subcortical voxel and cortical network. Voxel-wise results were highly similar ($r = 0.75$) between approaches using full correlations and partial correlations. We also repeated these procedures using the 15-networks Infomap solution (excluding unassigned vertices and medial temporal lobe vertices due to proximity to the subcortex; Fig. S8B left) as well as using a 7-network Infomap solution (Fig. S8A left).

In addition, we compared the correlation results against a null model using randomly rotated cortical networks, similar to (Gordon et al., 2017a; Gordon et al., 2016). First, for each subject we randomly rotated that subject's cortical networks around the spherical expansion of the cortical surface to produce cortical objects that had the same size, shape, and spatial distribution as real networks, but in random locations. Next, for every subcortical voxel, we calculated the average correlation to each rotated cortical network, excluding portions of the rotated networks that fell on the medial wall or in susceptibility artifact regions. This rotation and calculation of correlations was repeated 1000 times, generating a null distribution of correlations. Finally, for each network-subcortical voxel connection, we calculated the percent of iterations for which the correlation to the real network was stronger than the correlation to that iteration's rotated version of that network. This value represents the likelihood that a voxel's correlation to a cortical network is stronger than would be expected if the cortical network location was randomized. We compared this "percent

stronger than null" map to the standard functional connectivity correlation maps for each network for each subject.

Reliability of cortico-subcortical FC: Using an iterative split-half reliability analysis similar to (Gordon et al., 2017b; Laumann et al., 2015), we computed each individual subject's reliability of cortico-subcortical RSFC. For each subject, the ten scan sessions were randomly divided into two subsets of five sessions each. Half of the data (motion censored) was randomly selected from one of the subsets to serve as the comparison data, and a varying amount of data (5 to 100 minutes in 5 minute increments) was randomly selected from the other subset to serve as the test data. Reliability was estimated by computing the average correlation between the subcortical voxel-to-cortical network matrices for the comparison and test data. This procedure was iterated 1000 times using different subsets of random data (i.e., random halves of the data) in each iteration.

As some regions within the subcortex may have better reliability than others, we conducted a voxelwise split-half reliability analysis. For each subject, the ten scan sessions were randomized, concatenated, split into two halves, and the subcortical voxel-to-cortical network correlation matrices were computed for each half. Reliability for each voxel was estimated by computing the correlation between the halves. We also tested the relationship between reliability and tSNR by correlating these two measures across voxels for each subject. In order to mitigate the effects of voxels with relatively poor reliability, subsequent analyses excluded those voxels with reliability < .5 for each subject.

Task activations: Task fMRI data were processed as previously described (Gordon et al., 2017b; Gratton et al., 2018). Briefly, the cognitive/perceptual tasks consisted of a pair of mixed block/event-related design tasks that began with a task cue followed by a block of jittered trials in each task, modeled after Dubis et al. (2016). The "language" task trials consisted of single words and participants were asked to determine whether the words were nouns or verbs. The "perceptual" task consisted of Glass dot patterns (Glass, 1969) at either 50% or 0% coherence. Participants were asked to determine whether or not the dots were arranged concentrically. The motor task, modeled after the HCP motor task (Barch et al., 2013), consisted of blocks of movements of either left or right hand, left or right foot, or the tongue.

After standard fMRI preprocessing, task fMRI data were entered in a General Linear Model (GLM) separately for each session from each individual using in-house IDL software (FIDL) (Miezin et al., 2000). The mixed design tasks were modeled jointly in a single GLM with separate event regressors for onset and offset cues from each task, trials in each task (nouns and verbs for the cognitive task, 0% and 50% for the perceptual task), and a sustained block regressor for the task period. Event regressors were modeled using a finite impulse response approach consisting of delta functions at each of 8 timepoints, allowing for the more complete modeling of different HRF shapes (Ollinger et al., 2001). The motor task was modeled with separate block regressors for each motor condition.

Deactivations associated with the default mode network were identified using a contrast of the third and fourth timepoints from all conditions in the mixed design tasks (against an

implicit, unmodeled, baseline). Activations associated with the somatomotor hand network were identified using a contrast between left and right hand movement blocks with left and right foot movement blocks.

Similarity analysis: Similarity analyses were carried out similar to Gratton et al. (2018) and Marek et al. (2018). For each subject, the ten scan sessions were randomized, split into two halves, and concatenated. The subcortical voxel-to-cortical network correlation matrices were computed for each half and vectorized. Then the similarity (Pearson z(r)) between the two halves of data was calculated both within split halves of an individual's data and between split halves of every other individual. This analysis resulted in a similarity matrix, in which off-diagonal elements represent variance shared across individuals (i.e., group effect), and on-diagonal elements represent variance shared across scanning sessions within an individual. Variance unique to individuals vs. the group was quantified by normalizing (dividing) variance shared across individuals (group effect; off-diagonal elements) by subject similarity (on-diagonal elements). The production of similarity matrices and quantification of group vs. individual level effects were computed separately for the basal ganglia and thalamus.

We also examined between-subject variability in the subcortex as we have previously done in the cortex (Laumann et al., 2015) and cerebellum (Marek et al., 2018). We calculated the standard deviation of correlations between each subcortical voxel and every cortical network across subjects. We then assigned each subcortical voxel to a single network (standard winner-take-all approach) in order to compare the standard deviation of higher-order network subcortical voxels (frontoparietal, dorsal attention, ventral attention, salience, cingulo-opercular, default-mode) to that of processing network subcortical voxels (visual, somatomotor hand, somatomotor face) using a t-test.

Network specificity vs. integration: To determine which subcortical voxels were "network-specific" vs. "integrative" we implemented a modified winner-take-all analysis. For each subject, a "winning" network was assigned to each subcortical voxel based on the strength of the correlation between that voxel and each cortical network. The network with the strongest correlation was deemed the winner. Then, we categorized a voxel as network-specific if its correlations with all other networks were less than 2/3 (66.7%) of its correlation with the winning network, in line with Marek et al. (2018). If this criterion was not met, the voxel was categorized as integrative, and those networks within 2/3 of the winning network were also considered winners. This procedure yielded multiple networks (minimum two networks; maximum four networks – note that there was no instance with more than four networks) within an integrative voxel, whereas a network-specific voxel, by definition, was occupied by one network. Given the somewhat arbitrary nature of the 66.7% threshold, we also tested 50% and 75%, which resulted in highly similar distributions of network-specific vs. integrative functional zones (see Fig. S6A).

In addition, we tested an alternative approach for determining network specificity vs. integration based on effect size (Cohen's *d*). For every subcortical voxel, we computed t-tests comparing its correlations with the winning network (all cortical vertices within that network) to its correlations with every other network (all cortical vertices within a

subsequent network). Thus, we were able to compute the effect size of each comparison. Voxels were determined to be network-specific vs. integrative based on whether the observed effect size between the winning network and another network was greater than or less than a benchmarked effect size. In Fig. S6B, we show the resulting zones of integration for small ($d = 0.2$), medium ($d = 0.5$), and large ($d = 0.8$) effect sizes. This approach yielded similar zones of integration to the original approach described in the previous paragraph. Thus, our main results are reported using the original approach at a threshold of 66.7%.

Pictorially in Fig. 3, network-specific voxels were colored by their affiliated network, whereas integrative voxels were colored by each network represented in that voxel (striped pattern). For integrative voxels, the base color was determined by the network assigned to that voxel in separate, previously described group-averaged data (WashU 120) using a standard winner-take-all method (basal ganglia winner-take-all parcellations previously reported in Greene et al., 2014). Thus, if a network represented in an integrative voxel was shared with the network assigned to that voxel in the WashU 120, the voxel's base color was assigned to that network, and the other networks were shown as thin stripes. If none of the networks were shared with the WashU 120, the base color was assigned to the network with the strongest correlation.

One concern arising from delineating integration zones within the subcortex is the spatial proximity of networks given the relatively smaller size of subcortical structures. To lend support for integration zones rather than solely proximity to multiple networks, we performed a community density analysis across the subcortex. Using the winning network assignment for each subcortical voxel from the winner-take-all analysis, community density was determined by counting the number of networks within a spotlight of 3mm. If integration was largely due to high community density, the majority of high community density voxels would be expected to be integrative. To test this prediction, for each subject we extracted all voxels with a community density > 1, which indicates the presence of at least one neighboring voxel with a different network assignment, and calculated the percent of those voxels that were integrative.

Quantification of network-specificity and integration across functional networks: To examine how network-specificity and integration were distributed across functional networks, we quantified the number of network-specific and integrative voxels for each network. We generated a network-by-network matrix representing the number of voxels, summed across subjects, that were integrative for all pairs of networks (e.g., number of integrative voxels containing frontoparietal and salience networks). We normalized these summed values by the total number of integrative voxels, resulting in a percentage of integrative voxels for each network combination. We calculated these percentages separately for each structure. We determined the degree to which functional networks cluster with respect to patterns of integration (i.e., extent to which certain networks preferentially integrated with each other). To this end, we performed a hierarchical clustering analysis using Matlab's *linkage, pdist,* and *dendrogram* functions, with default setting for determining the optimal cluster solution. We validated the clusters produced by the hierarchical clustering analysis by submitting the network-by-network matrix to a graph

theoretic clustering analysis (modularity) (Newman, 2006), replicating a three cluster solution.

Defining functional zones in the subcortex: Having determined network-specific and integrative subcortical voxels for each subject, we aimed to identify zones of network-specificity and integration that were common across the group vs. variable across individuals. First, a voxel was considered network-specific if that voxel was network-specific in > 5 subjects. A voxel was considered integrative if that voxel was integrative in > 5 subjects. If a voxel met neither criteria, it was not assigned to a zone. For the assigned voxels, we next determined whether they exhibited RSFC that was common across the group (Group) or varied across individuals (Individual). For network-specific voxels, they were considered Group if > 5 subjects shared the same network assignment; otherwise, they were considered Individual. For integrative voxels, they were considered Group if at least two of the networks assigned to that voxel were present in > 5 subjects; otherwise, they were considered Individual. Thus, we defined four voxel types: Group Network-specific, Group Integrative, Individual Network-specific, and Individual Integrative. To delineate functional zones, we applied a cluster threshold of 20 voxels and removed extraneous voxels that did not share more than one face with other voxels in that cluster, i.e. ensuring a Euler characteristic of two (Worsley, 1996).

To determine the stability of these functional zones, we performed a jack-knifing procedure. The steps just described for defining the four zones were repeated ten times, leaving out a unique subject with each iteration. We then calculated the percent of iterations that each voxel was assigned to each of the four zone types. Thus, we estimated confidence in functional zone assignment (Fig. 6A).

Functional zone examples: To display examples of each of the four types of functional zones, we selected an example voxel within each type (Fig. 6A). Fig. 6B displays the correlations from these voxels to all cortical vertices on the cortical surface with subject-specific Infomap network borders for two representative subjects, as well as the strength of the correlations to each cortical network.

DATA AND SOFTWARE AVAILABILITY

The “Midnight Scan Club” data (raw and processed) used in the present study are available in the OpenfMRI data repository at https://openfmri.org/dataset/ds000224/. Processing and analysis code is available at https://github.com/MidnightScanClub/MSCcodebase.

Supplementary Material

Refer to Web version on PubMed Central for supplementary material.

ACKNOWLEDGEMENTS

This work was supported by NIH grants MH104592 (DJG), MH100019 (SM), NS088590 (NUFD), MH100872 (TOL), MH112473 (TOL), MH002920 (AWG), NS110332 (DJN), 1P30NS098577 (to NIAC), and HD087011 (to IDDRC at WU); Jacobs Foundation grant 2016121703 (NUFD); Child Neurology Foundation (NUFD); McDonnell Center for Systems Neuroscience (DJG, NUFD, BLS); Hope Center for Neurological Disorders (NUFD, BLS, SEP); and US Department of Veterans Affairs Clinical Sciences Research and Development Service grant

1IK2CX001680 (EMG). The views expressed in this article are those of the authors and do not necessarily reflect the position or policy of the Department of Veterans Affairs or the US government.

REFERENCES

Albin RL, Young AB, and Penney JB (1989). The functional anatomy of basal ganglia disorders. Trends Neurosci 12, 366–375. [PubMed: 2479133]

Alexander GE, and Crutcher MD (1990a). Basal ganglia-thalamocortical circuits: parallel substrates for motor,oculomotor,prefrontal and limbic functions. Prog Brain Res 85, 119–146. [PubMed: 2094891]

Alexander GE, and Crutcher MD (1990b). Functional architecture of basal ganglia circuits: neural substrates of parallel processing. Trends Neurosci 13, 266–271. [PubMed: 1695401]

Alexander GE, Delong MR, and Strick PL (1986). Parallel organization of functionally segregated circuits linking basal ganglia and cortex. Annu Rev Neurosci 9, 357–381. [PubMed: 3085570]

Alhourani A, McDowell MM, Randazzo MJ, Wozny TA, Kondylis ED, Lipski WJ, Beck S, Karp JF, Ghuman AS, and Richardson RM (2015). Network effects of deep brain stimulation. J Neurophysiol 114, 2105–2117. [PubMed: 26269552]

Argall BD, Saad ZS, and Beauchamp MS (2006). Simplified intersubject averaging on the cortical surface using SUMA. Hum Brain Mapp 27, 14–27. [PubMed: 16035046]

Arsalidou M, Duerden EG, and Taylor MJ (2013). The centre of the brain: topographical model of motor, cognitive, affective, and somatosensory functions of the basal ganglia. Hum Brain Mapp 34, 3031–3054. [PubMed: 22711692]

Averbeck BB, Lehman J, Jacobson M, and Haber SN (2014). Estimates of projection overlap and zones of convergence within frontal-striatal circuits. J Neurosci 34, 9497–9505. [PubMed: 25031393]

Baizabal-Carvallo JF, Kagnoff MN, Jimenez-Shahed J, Fekete R, and Jankovic J (2014). The safety and efficacy of thalamic deep brain stimulation in essential tremor: 10 years and beyond. J Neurol Neurosurg Psychiatry 85, 567–572. [PubMed: 24096713]

Balota DA, Yap MJ, Cortese MJ, Hutchison KA, Kessler B, Loftis B, Neely JH, Nelson DL, Simpson GB, and Treiman R (2007). The English Lexicon Project. Behav Res Methods 39, 445–459. [PubMed: 17958156]

Barch DM, Burgess GC, Harms MP, Petersen SE, Schlaggar BL, Corbetta M, Glasser MF, Curtiss S, Dixit S, Feldt C, et al. (2013). Function in the human connectome: Task-fMRI and individual differences in behavior. Neuroimage.

Barnes KA, Cohen AL, Power JD, Nelson SM, Miezin FM, Petersen SE, and Schlaggar BL (2010). Identifying basal ganglia divisions in individuals using resting-state functional connectivity MRI. Frontiers in Systems Neuroscience 4, 18. [PubMed: 20589235]

Behrens TE, Johansen-Berg H, Woolrich MW, Smith SM, Wheeler-Kingshott CA, Boulby PA, Barker GJ, Sillery EL, Sheehan K, Ciccarelli O, et al. (2003). Non-invasive mapping of connections between human thalamus and cortex using diffusion imaging. Nat Neurosci 6, 750–757. [PubMed: 12808459]

Behzadi Y, Restom K, Liau J, and Liu TT (2007). A component based noise correction method (CompCor) for BOLD and perfusion based fMRI. Neuroimage 37, 90–101. [PubMed: 17560126]

Bogousslavsky J, Regli F, and Uske A (1988). Thalamic infarcts: clinical syndromes, etiology, and prognosis. Neurology 38, 837–848. [PubMed: 3368064]

Bosch-Bouju C, Hyland BI, and Parr-Brownlie LC (2013). Motor thalamus integration of cortical, cerebellar and basal ganglia information: implications for normal and parkinsonian conditions. Front Comput Neurosci 7, 163. [PubMed: 24273509]

Bostan AC, and Strick PL (2018). The basal ganglia and the cerebellum: nodes in an integrated network. Nat Rev Neurosci 19, 338–350. [PubMed: 29643480]

Bot M, Schuurman PR, Odekerken VJJ, Verhagen R, Contarino FM, De Bie RMA, and van den Munckhof P (2018). Deep brain stimulation for Parkinson's disease: defining the optimal location within the subthalamic nucleus. J Neurol Neurosurg Psychiatry 89, 493–498. [PubMed: 29353236]

Bradshaw JL, and Sheppard DM (2000). The neurodevelopmental frontostriatal disorders: evolutionary adaptiveness and anomalous lateralization. Brain Lang 73, 297–320. [PubMed: 10856179]

Braga RM, and Buckner RL (2017). Parallel Interdigitated Distributed Networks within the Individual Estimated by Intrinsic Functional Connectivity. Neuron 95, 457–471 e455. [PubMed: 28728026]

Campbell MC, Black KJ, Weaver PM, Lugar HM, Videen TO, Tabbal SD, Karimi M, Perlmutter JS, and Hershey T (2012). Mood response to deep brain stimulation of the subthalamic nucleus in Parkinson's disease. J Neuropsychiatry Clin Neurosci 24, 28–36. [PubMed: 22450611]

Campbell MC, Karimi M, Weaver PM, Wu J, Perantie DC, Golchin NA, Tabbal SD, Perlmutter JS, and Hershey T (2008). Neural correlates of STN DBS-induced cognitive variability in Parkinson disease. Neuropsychologia 46, 3162–3169. [PubMed: 18682259]

Choi EY, Tanimura Y, Vage PR, Yates EH, and Haber SN (2017). Convergence of prefrontal and parietal anatomical projections in a connectional hub in the striatum. Neuroimage 146, 821–832. [PubMed: 27646127]

Choi EY, Yeo BT, and Buckner RL (2012). The organization of the human striatum estimated by intrinsic functional connectivity. J Neurophysiol 108, 2242–2263. [PubMed: 22832566]

Ciric R, Wolf DH, Power JD, Roalf DR, Baum GL, Ruparel K, Shinohara RT, Elliott MA, Eickhoff SB, Davatzikos C, et al. (2017). Benchmarking of participant-level confound regression strategies for the control of motion artifact in studies of functional connectivity. Neuroimage 154, 174–187. [PubMed: 28302591]

Corbetta M, Ramsey L, Callejas A, Baldassarre A, Hacker CD, Siegel JS, Astafiev SV, Rengachary J, Zinn K, Lang CE, et al. (2015). Common behavioral clusters and subcortical anatomy in stroke. Neuron 85, 927–941. [PubMed: 25741721]

Corbetta M, and Shulman GL (2002). Control of goal-directed and stimulus-driven attention in the brain. Nature Reviews Neuroscience 3, 201–215. [PubMed: 11994752]

Crittenden BM, Mitchell DJ, and Duncan J (2016). Task Encoding across the Multiple Demand Cortex Is Consistent with a Frontoparietal and Cingulo-Opercular Dual Networks Distinction. J Neurosci 36, 6147–6155. [PubMed: 27277793]

Dale AM, Fischl B, and Sereno MI (1999). Cortical surface-based analysis. I. Segmentation and surface reconstruction. Neuroimage 9, 179–194. [PubMed: 9931268]

Damoiseaux JS, Rombouts SA, Barkhof F, Scheltens P, Stam CJ, Smith SM, and Beckmann CF (2006). Consistent resting-state networks across healthy subjects. Proc Natl Acad Sci U S A 103, 13848–13853. [PubMed: 16945915]

Dandekar MP, Fenoy AJ, Carvalho AF, Soares JC, and Quevedo J (2018). Deep brain stimulation for treatment-resistant depression: an integrative review of preclinical and clinical findings and translational implications. Mol Psychiatry 23, 1094–1112. [PubMed: 29483673]

Di Martino A, Scheres A, Margulies DS, Kelly AMC, Uddin LQ, Shehzad Z, Biswal B, Walters JR, Castellanos FX, and Milham MP (2008). Functional connectivity of human striatum: a resting state FMRI study. Cereb Cortex 18, 2735–2747. [PubMed: 18400794]

Dosenbach NUF (2008). Human Task Control Systems In Neurology (Saint Louis, MO, Washington University), p. 233.

Dosenbach NUF, Fair DA, Cohen AL, Schlaggar BL, and Petersen SE (2008). A dual-networks architecture of top-down control. Trends Cogn Sci 12, 99–105. [PubMed: 18262825]

Dosenbach NUF, Fair DA, Miezin FM, Cohen AL, Wenger KK, Dosenbach RAT, Fox MD, Snyder AZ, Vincent JL, Raichle ME, et al. (2007). Distinct brain networks for adaptive and stable task control in humans. Proc Natl Acad Sci U S A 104, 11073–11078. [PubMed: 17576922]

Dosenbach NUF, Visscher KM, Palmer ED, Miezin FM, Wenger KK, Kang HC, Burgund ED, Grimes AL, Schlaggar BL, and Petersen SE (2006). A core system for the implementation of task sets. Neuron 50, 799–812. [PubMed: 16731517]

Draganski B, Kherif F, Kloppel S, Cook PA, Alexander DC, Parker GJ, Deichmann R, Ashburner J, and Frackowiak RS (2008). Evidence for segregated and integrative connectivity patterns in the human Basal Ganglia. J Neurosci 28, 7143–7152. [PubMed: 18614684]

Drysdale AT, Grosenick L, Downar J, Dunlop K, Mansouri F, Meng Y, Fetcho RN, Zebley B, Oathes DJ, Etkin A, et al. (2017). Resting-state connectivity biomarkers define neurophysiological subtypes of depression. Nat Med 23, 28–38. [PubMed: 27918562]

Dubis JW, Siegel JS, Neta M, Visscher KM, and Petersen SE (2016). Tasks Driven by Perceptual Information Do Not Recruit Sustained BOLD Activity in Cingulo-Opercular Regions. Cereb Cortex 26, 192–201. [PubMed: 25150283]

Dum RP, and Strick PL (1993). Cingulate motor areas In Neurobiology of cingulate cortex and limbic thalamus: a comprehensive handbook, Vogt BA, and Gabriel M, eds. (Boston, MA: Birkhauser), pp. 415–441.

Duncan J, and Owen AM (2000). Common regions of the human frontal lobe recruited by diverse cognitive demands. Trends Neurosci 23, 475–483. [PubMed: 11006464]

Fair DA, Bathula D, Mills KL, Dias TG, Blythe MS, Zhang D, Snyder AZ, Raichle ME, Stevens AA, Nigg JT, and Nagel BJ (2010). Maturing thalamocortical functional connectivity across development. Front Syst Neurosci 4, 10. [PubMed: 20514143]

Filevich E, Lisofsky N, Becker M, Butler O, Lochstet M, Martensson J, Wenger E, Lindenberger U, and Kuhn S (2017). Day2day: investigating daily variability of magnetic resonance imaging measures over half a year. BMC Neurosci 18, 65. [PubMed: 28836958]

Finn ES, Shen X, Scheinost D, Rosenberg MD, Huang J, Chun MM, Papademetris X, and Constable RT (2015). Functional connectome fingerprinting: identifying individuals using patterns of brain connectivity. Nat Neurosci 18, 1664–1671. [PubMed: 26457551]

Fischer J, and Whitney D (2012). Attention gates visual coding in the human pulvinar. Nat Commun 3, 1051. [PubMed: 22968697]

Fischl B (2012). FreeSurfer. Neuroimage 62, 774–781. [PubMed: 22248573]

Fischl B, Sereno MI, and Dale AM (1999). Cortical surface-based analysis. II: Inflation, flattening, and a surface-based coordinate system. Neuroimage 9, 195–207. [PubMed: 9931269]

Fox MD, Buckner RL, Liu H, Chakravarty MM, Lozano AM, and Pascual-Leone A (2014). Resting-state networks link invasive and noninvasive brain stimulation across diverse psychiatric and neurological diseases. Proc Natl Acad Sci U S A 111, E4367–4375. [PubMed: 25267639]

Friston KJ, Williams S, Howard R, Frackowiak RS, and Turner R (1996). Movement-related effects in fMRI time-series. Magn Reson Med 35, 346–355. [PubMed: 8699946]

Garcia-Garcia M, Nikolaidis A, Bellec P, Craddock RC, Cheung B, Castellanos FX, and Milham MP (2017). Detecting stable individual differences in the functional organization of the human basal ganglia. Neuroimage.

Garrett DD, Epp SM, Perry A, and Lindenberger U (2018). Local temporal variability reflects functional integration in the human brain. Neuroimage 183, 776–787. [PubMed: 30149140]

Glass L (1969). Moire effect from random dots. Nature 223, 578–580. [PubMed: 5799528]

Glasser MF, Coalson TS, Robinson EC, Hacker CD, Harwell J, Yacoub E, Ugurbil K, Andersson J, Beckmann CF, Jenkinson M, et al. (2016). A multi-modal parcellation of human cerebral cortex. Nature 536, 171–178. [PubMed: 27437579]

Gordon EM, Laumann TO, Adeyemo B, Gilmore AW, Nelson SM, Dosenbach NU, and Petersen SE (2017a). Individual-specific features of brain systems identified with resting state functional correlations. Neuroimage 146, 918–939. [PubMed: 27640749]

Gordon EM, Laumann TO, Adeyemo B, Huckins JF, Kelley WM, and Petersen SE (2016). Generation and Evaluation of a Cortical Area Parcellation from Resting-State Correlations. Cereb Cortex 26, 288–303. [PubMed: 25316338]

Gordon EM, Laumann TO, Gilmore AW, Newbold DJ, Greene DJ, Berg JJ, Ortega M, Hoyt-Drazen C, Gratton C, Sun H, et al. (2017b). Precision Functional Mapping of Individual Human Brains. Neuron 95, 791–807 e797. [PubMed: 28757305]

Gordon EM, Lynch CJ, Gratton C, Laumann TO, Gilmore AW, Greene DJ, Ortega M, Nguyen AL, Schlaggar BL, Petersen SE, et al. (2018). Three Distinct Sets of Connector Hubs Integrate Human Brain Function. Cell Rep 24, 1687–1695 e1684. [PubMed: 30110625]

Gratton C, Laumann TO, Nielsen AN, Greene DJ, Gordon EM, Gilmore AW, Nelson SM, Coalson RS, Snyder AZ, Schlaggar BL, et al. (2018). Functional Brain Networks Are Dominated by Stable Group and Individual Factors, Not Cognitive or Daily Variation. Neuron 98, 439–452 e435. [PubMed: 29673485]

Gratton C, Neta M, Sun H, Ploran EJ, Schlaggar BL, Wheeler ME, Petersen SE, and Nelson SM (2017). Distinct Stages of Moment-to-Moment Processing in the Cinguloopercular and Frontoparietal Networks. Cereb Cortex 27, 2403–2417. [PubMed: 27095824]

Greene DJ, Laumann TO, Dubis JW, Ihnen SK, Neta M, Power JD, Pruett JR Jr., Black KJ, and Schlaggar BL (2014). Developmental changes in the organization of functional connections between the basal ganglia and cerebral cortex. J Neurosci 34, 5842–5854. [PubMed: 24760844]

Greene DJ, Williams Iii AC, Koller JM, Schlaggar BL, and Black KJ (2017). Brain structure in pediatric Tourette syndrome. Mol Psychiatry 22, 972–980. [PubMed: 27777415]

Grillner S, Robertson B, and Stephenson-Jones M (2013). The evolutionary origin of the vertebrate basal ganglia and its role in action selection. J Physiol 591, 5425–5431. [PubMed: 23318875]

Haber SN (2003). The primate basal ganglia: parallel and integrative networks. J Chem Neuroanat 26, 317–330. [PubMed: 14729134]

Haber SN (2016). Corticostriatal circuitry. Dialogues Clin Neurosci 18, 7–21. [PubMed: 27069376]

He Y, and Evans A (2010). Graph theoretical modeling of brain connectivity. Curr Opin Neurol 23, 341–350. [PubMed: 20581686]

Heller AS (2016). Cortical-Subcortical Interactions in Depression: From Animal Models to Human Psychopathology. Front Syst Neurosci 10, 20. [PubMed: 27013988]

Hershey T, Campbell MC, Videen TO, Lugar HM, Weaver PM, Hartlein J, Karimi M, Tabbal SD, and Perlmutter JS (2010). Mapping Go-No-Go performance within the subthalamic nucleus region. Brain 133, 3625–3634. [PubMed: 20855421]

Horien C, Shen X, Scheinost D, and Constable RT (2019). The individual functional connectome is unique and stable over months to years. Neuroimage 189, 676–687. [PubMed: 30721751]

Horn A (2019). The impact of modern-day neuroimaging on the field of deep brain stimulation. Curr Opin Neurol 32, 511–520. [PubMed: 30844863]

Horn A, Li N, Dembek TA, Kappel A, Boulay C, Ewert S, Tietze A, Husch A, Perera T, Neumann WJ, et al. (2019). Lead-DBS v2: Towards a comprehensive pipeline for deep brain stimulation imaging. Neuroimage 184, 293–316. [PubMed: 30179717]

Houeto JL, Mesnage V, Welter ML, Mallet L, Agid Y, and Bejjani BP (2003). Subthalamic DBS replaces levodopa in Parkinson's disease: two-year follow-up. Neurology 60, 154–155; author reply 154-155.

Hwang K, Bertolero MA, Liu WB, and D'Esposito M (2017). The Human Thalamus Is an Integrative Hub for Functional Brain Networks. J Neurosci 37, 5594–5607. [PubMed: 28450543]

Janssen RJ, Jylanki P, Kessels RP, and van Gerven MA (2015). Probabilistic model-based functional parcellation reveals a robust, fine-grained subdivision of the striatum. Neuroimage 119, 398–405. [PubMed: 26163800]

Jarbo K, and Verstynen TD (2015). Converging structural and functional connectivity of orbitofrontal, dorsolateral prefrontal, and posterior parietal cortex in the human striatum. J Neurosci 35, 3865–3878. [PubMed: 25740516]

Jones EG (1998). Viewpoint: the core and matrix of thalamic organization. Neuroscience 85, 331–345. [PubMed: 9622234]

Kastner S, and Pinsk MA (2004). Visual attention as a multilevel selection process. Cogn Affect Behav Neurosci 4, 483–500. [PubMed: 15849892]

Laumann TO, Gordon EM, Adeyemo B, Snyder AZ, Joo SJ, Chen MY, Gilmore AW, McDermott KB, Nelson SM, Dosenbach NU, et al. (2015). Functional System and Areal Organization of a Highly Sampled Individual Human Brain. Neuron 87, 657–670. [PubMed: 26212711]

Leh SE, Chakravarty MM, and Ptito A (2008). The connectivity of the human pulvinar: a diffusion tensor imaging tractography study. Int J Biomed Imaging 2008, 789539. [PubMed: 18274667]

Lehericy S, Ducros M, Van de Moortele PF, Francois C, Thivard L, Poupon C, Swindale N, Ugurbil K, and Kim DS (2004). Diffusion tensor fiber tracking shows distinct corticostriatal circuits in humans. Ann Neurol 55, 522–529. [PubMed: 15048891]

Liston C, Malter Cohen M, Teslovich T, Levenson D, and Casey BJ (2011). Atypical prefrontal connectivity in attention-deficit/hyperactivity disorder: pathway to disease or pathological end point? Biol Psychiatry 69, 1168–1177. [PubMed: 21546000]

Luking KR, Pagliaccio D, Luby JL, and Barch DM (2016). Reward Processing and Risk for Depression Across Development. Trends Cogn Sci 20, 456–468. [PubMed: 27131776]

Mandat TS, Hurwitz T, and Honey CR (2006). Hypomania as an adverse effect of subthalamic nucleus stimulation: report of two cases. Acta Neurochir (Wien) 148, 895–897; discussion 898. [PubMed: 16763733]

Marcus DS, Harwell J, Olsen T, Hodge M, Glasser MF, Prior F, Jenkinson M, Laumann T, Curtiss SW, and Van Essen DC (2011). Informatics and data mining tools and strategies for the human connectome project. Front Neuroinform 5, 4. [PubMed: 21743807]

Marek S, Hwang K, Foran W, Hallquist MN, and Luna B (2015). The Contribution of Network Organization and Integration to the Development of Cognitive Control. PLoS Biol 13, e1002328. [PubMed: 26713863]

Marek S, Siegel JS, Gordon EM, Raut RV, Gratton C, Newbold DJ, Ortega M, Laumann TO, Adeyemo B, Miller DB, et al. (2018). Spatial and Temporal Organization of the Individual Human Cerebellum. Neuron 100, 977–993 e977. [PubMed: 30473014]

McIntyre CC, and Hahn PJ (2010). Network perspectives on the mechanisms of deep brain stimulation. Neurobiol Dis 38, 329–337. [PubMed: 19804831]

Metzger CD, van der Werf YD, and Walter M (2013). Functional mapping of thalamic nuclei and their integration into cortico-striatal-thalamo-cortical loops via ultra-high resolution imaging-from animal anatomy to in vivo imaging in humans. Front Neurosci 7, 24. [PubMed: 23658535]

Miezin F, Maccotta L, Ollinger JM, Petersen SE, and Buckner RL (2000). Characterizing the hemodynamic response: effects of presentation rate, sampling procedure, and the possibility of ordering brain activity based on relative timing. Neuroimage 11, 735–759. [PubMed: 10860799]

Mink JW (2001). Basal ganglia dysfunction in Tourette's syndrome: a new hypothesis. Pediatr Neurol 25, 190–198. [PubMed: 11587872]

Mink JW (2003). The Basal Ganglia and involuntary movements: impaired inhibition of competing motor patterns. ArchNeurol 60, 1365–1368.

Mink JW (2009). Clinical review of DBS for Tourette Syndrome. Front Biosci (Elite Ed) 1, 72–76. [PubMed: 19482626]

Miranda-Dominguez O, Mills BD, Carpenter SD, Grant KA, Kroenke CD, Nigg JT, and Fair DA (2014). Connectotyping: model based fingerprinting of the functional connectome. PLoS One 9, e111048. [PubMed: 25386919]

Mueller S, Wang D, Fox MD, Yeo BT, Sepulcre J, Sabuncu MR, Shafee R, Lu J, and Liu H (2013). Individual variability in functional connectivity architecture of the human brain. Neuron 77, 586–595. [PubMed: 23395382]

Nelson SM, Dosenbach NU, Cohen AL, Wheeler ME, Schlaggar BL, and Petersen SE (2010). Role of the anterior insula in task-level control and focal attention. Brain Struct Funct 214, 669–680. [PubMed: 20512372]

Nestor KA, Jones JD, Butson CR, Morishita T, Jacobson C.E.t., Peace DA, Chen D, Foote KD, and Okun MS (2014). Coordinate-based lead location does not predict Parkinson's disease deep brain stimulation outcome. PLoS One 9, e93524. [PubMed: 24691109]

Neta M, Miezin FM, Nelson SM, Dubis JW, Dosenbach NU, Schlaggar BL, and Petersen SE (2015). Spatial and temporal characteristics of error-related activity in the human brain. J Neurosci 35, 253–266. [PubMed: 25568119]

Newman ME (2006). Modularity and community structure in networks. Proc Natl Acad Sci U S A 103, 8577–8582. [PubMed: 16723398]

Noble S, Spann MN, Tokoglu F, Shen X, Constable RT, and Scheinost D (2017). Influences on the Test-Retest Reliability of Functional Connectivity MRI and its Relationship with Behavioral Utility. Cereb Cortex 27, 5415–5429. [PubMed: 28968754]

Ollinger JM, Corbetta M, and Shulman GL (2001). Separating processes within a trial in event-related functional MRI II. Analysis. Neuroimage 13, 218–229. [PubMed: 11133324]

Ondo W, Jankovic J, Schwartz K, Almaguer M, and Simpson RK (1998). Unilateral thalamic deep brain stimulation for refractory essential tremor and Parkinson's disease tremor. Neurology 51, 1063–1069. [PubMed: 9781530]

Patriat R, Molloy EK, and Birn RM (2015). Using Edge Voxel Information to Improve Motion Regression for rs-fMRI Connectivity Studies. Brain Connect 5, 582–595. [PubMed: 26107049]

Perlmutter JS, and Mink JW (2006). Deep brain stimulation. Annu Rev Neurosci 29, 229–257. [PubMed: 16776585]

Perriol MP, Krystkowiak P, Defebvre L, Blond S, Destee A, and Dujardin K (2006). Stimulation of the subthalamic nucleus in Parkinson's disease: cognitive and affective changes are not linked to the motor outcome. Parkinsonism Relat Disord 12, 205–210. [PubMed: 16549386]

Petersen SE, and Posner MI (2012). The attention system of the human brain: 20 years after. Annu Rev Neurosci 35, 73–89. [PubMed: 22524787]

Petersen SE, Robinson DL, and Keys W (1985). Pulvinar nuclei of the behaving rhesus monkey: Visual responses and their modulation. J Neurophysiol 54, 867–886. [PubMed: 4067625]

Petersen SE, Robinson DL, and Morris JD (1987). Contributions of the pulvinar to visual spatial attention. Neuropsychologia 25, 97–105. [PubMed: 3574654]

Poldrack RA, Laumann TO, Koyejo O, Gregory B, Hover A, Chen MY, Gorgolewski KJ, Luci J, Joo SJ, Boyd RL, et al. (2015). Long-term neural and physiological phenotyping of a single human. Nat Commun 6, 8885. [PubMed: 26648521]

Power JD, Cohen AL, Nelson SM, Wig GS, Barnes KA, Church JA, Vogel AC, Laumann TO, Miezin FM, Schlaggar BL, and Petersen SE (2011). Functional network organization of the human brain. Neuron 72, 665–678. [PubMed: 22099467]

Power JD, Mitra A, Laumann TO, Snyder AZ, Schlaggar BL, and Petersen SE (2014). Methods to detect, characterize, and remove motion artifact in resting state fMRI. Neuroimage 84, 320–341. [PubMed: 23994314]

Power JD, Schlaggar BL, Lessov-Schlaggar CN, and Petersen SE (2013). Evidence for hubs in human functional brain networks. Neuron 79, 798–813. [PubMed: 23972601]

Raut RV, Mitra A, Snyder AZ, and Raichle ME (2019). On time delay estimation and sampling error in resting-state fMRI. Neuroimage 194, 211–227. [PubMed: 30902641]

Righi G, Peissig JJ, and Tarr MJ (2012). Recognizing disguised faces. Vis Cogn 20, 143–169.

Ring HA, and Serra-Mestres J (2002). Neuropsychiatry of the basal ganglia. J Neurol Neurosurg Psychiatry 72, 12–21. [PubMed: 11784818]

Rinne P, Hassan M, Fernandes C, Han E, Hennessy E, Waldman A, Sharma P, Soto D, Leech R, Malhotra PA, and Bentley P (2018). Motor dexterity and strength depend upon integrity of the attention-control system. Proc Natl Acad Sci U S A 115, E536–E545. [PubMed: 29284747]

Rosvall M, and Bergstrom CT (2008). Maps of random walks on complex networks reveal community structure. Proc Natl Acad Sci U S A 105, 1118–1123 %U http://www.ncbi.nlm.nih.gov.beckerproxy.wustl.edu/pubmed/18216267. [PubMed: 18216267]

Saalmann YB, Pinsk MA, Wang L, Li X, and Kastner S (2012). The pulvinar regulates information transmission between cortical areas based on attention demands. Science 337, 753–756. [PubMed: 22879517]

Sadaghiani S, and D'Esposito M (2015). Functional Characterization of the Cingulo-Opercular Network in the Maintenance of Tonic Alertness. Cereb Cortex 25, 2763–2773. [PubMed: 24770711]

Satterthwaite TD, Elliott MA, Gerraty RT, Ruparel K, Loughead J, Calkins ME, Eickhoff SB, Hakonarson H, Gur RC, Gur RE, and Wolf DH (2013). An improved framework for confound regression and filtering for control of motion artifact in the preprocessing of resting-state functional connectivity data. Neuroimage 64, 240–256. [PubMed: 22926292]

Seitzman BA, Gratton C, Laumann TO, Gordon EM, Adeyemo B, Dworetsky A, Kraus BT, Gilmore AW, Berg JJ, Ortega M, et al. (2019). Trait-like variants in human functional brain networks. Proc Natl Acad Sci U S A 116, 22851–22861. [PubMed: 31611415]

Selemon LD, and Goldman-Rakic PS (1985). Longitudinal topography and interdigitation of corticostriatal projections in the rhesus monkey. J Neurosci 5, 776–794. [PubMed: 2983048]

Shipp S (2001). Corticopulvinar connections of areas V5, V4, and V3 in the macaque monkey: a dual model of retinal and cortical topographies. J Comp Neurol 439, 469–490. [PubMed: 11596067]

Shipp S (2004). The brain circuitry of attention. Trends Cogn Sci 8, 223–230. [PubMed: 15120681]

Siegel JS, Snyder AZ, Metcalf NV, Fucetola RP, Hacker CD, Shimony JS, Shulman GL, and Corbetta M (2014). The circuitry of abulia: insights from functional connectivity MRI. Neuroimage Clin 6, 320–326. [PubMed: 25379445]

Skogseid IM (2014). Dystonia--new advances in classification, genetics, pathophysiology and treatment. Acta Neurol Scand Suppl, 13–19. [PubMed: 24588501]

Smith SM, Jenkinson M, Woolrich MW, Beckmann CF, Behrens TE, Johansen-Berg H, Bannister PR, De Luca M, Drobnjak I, Flitney DE, et al. (2004). Advances in functional and structural MR image analysis and implementation as FSL. Neuroimage 23 Suppl 1, S208–S219. [PubMed: 15501092]

Starr PA, Turner RS, Rau G, Lindsey N, Heath S, Volz M, Ostrem JL, and Marks WJ Jr. (2006). Microelectrode-guided implantation of deep brain stimulators into the globus pallidus internus for dystonia: techniques, electrode locations, and outcomes. J Neurosurg 104, 488–501. [PubMed: 16619651]

Tolleson C, Pallavaram S, Li C, Fang J, Phibbs F, Konrad P, Hedera P, D'Haese PF, Dawant BM, and Davis TL (2015). The optimal pallidal target in deep brain stimulation for dystonia: a study using a functional atlas based on nonlinear image registration. Stereotact Funct Neurosurg 93, 17–24. [PubMed: 25502118]

Van Essen DC (2005). A Population-Average, Landmark- and Surface-based (PALS) Atlas of Human Cerebral Cortex. Neuroimage 28, 635–662. [PubMed: 16172003]

Van Essen DC, Glasser MF, Dierker DL, Harwell J, and Coalson T (2012). Parcellations and hemispheric asymmetries of human cerebral cortex analyzed on surface-based atlases. Cereb Cortex 22, 2241–2262. [PubMed: 22047963]

van Westen M, Rietveld E, Figee M, and Denys D (2015). Clinical Outcome and Mechanisms of Deep Brain Stimulation for Obsessive-Compulsive Disorder. Curr Behav Neurosci Rep 2, 41–48. [PubMed: 26317062]

Vidailhet M, Vercueil L, Houeto JL, Krystkowiak P, Benabid AL, Cornu P, Lagrange C, Tezenas du Montcel S, Dormont D, Grand S, et al. (2005). Bilateral deep-brain stimulation of the globus pallidus in primary generalized dystonia. N Engl J Med 352, 459–467. [PubMed: 15689584]

Weller RE, Steele GE, and Kaas JH (2002). Pulvinar and other subcortical connections of dorsolateral visual cortex in monkeys. J Comp Neurol 450, 215–240. [PubMed: 12209852]

Wichmann T, and Delong MR (2011). Deep-Brain Stimulation for Basal Ganglia Disorders. Basal Ganglia 1, 65–77. [PubMed: 21804953]

Wodarg F, Herzog J, Reese R, Falk D, Pinsker MO, Steigerwald F, Jansen O, Deuschl G, Mehdorn HM, and Volkmann J (2012). Stimulation site within the MRI-defined STN predicts postoperative motor outcome. Mov Disord 27, 874–879. [PubMed: 22517070]

Worsley KJ (1996). The geometry of random images. Chance 9, 27–40.

Yan CG, Cheung B, Kelly C, Colcombe S, Craddock RC, Di Martino A, Li Q, Zuo XN, Castellanos FX, and Milham MP (2013). A comprehensive assessment of regional variation in the impact of head micromovements on functional connectomics. Neuroimage 76, 183–201. [PubMed: 23499792]

Yeo BT, Krienen FM, Sepulcre J, Sabuncu MR, Lashkari D, Hollinshead M, Roffman JL, Smoller JW, Zollei L, Polimeni JR, et al. (2011). The organization of the human cerebral cortex estimated by intrinsic functional connectivity. J Neurophysiol 106, 1125–1165. [PubMed: 21653723]

Zaaroor M, Sinai A, Goldsher D, Eran A, Nassar M, and Schlesinger I (2018). Magnetic resonance-guided focused ultrasound thalamotomy for tremor: a report of 30 Parkinson's disease and essential tremor cases. J Neurosurg 128, 202–210. [PubMed: 28298022]

Zhang D, Snyder AZ, Fox MD, Sansbury MW, Shimony JS, and Raichle ME (2008). Intrinsic functional relations between human cerebral cortex and thalamus. J Neurophysiol 100, 1740–1748. [PubMed: 18701759]

Highlights

- We identify human subcortical integration zones using precision function mapping
- Systematic connectivity reveals motor, cognitive & visual attention integration zones
- Subcortical functional organization has individually-variable & conserved features
- Integration zones map onto variably effective DBS sites, suggesting clinical utility

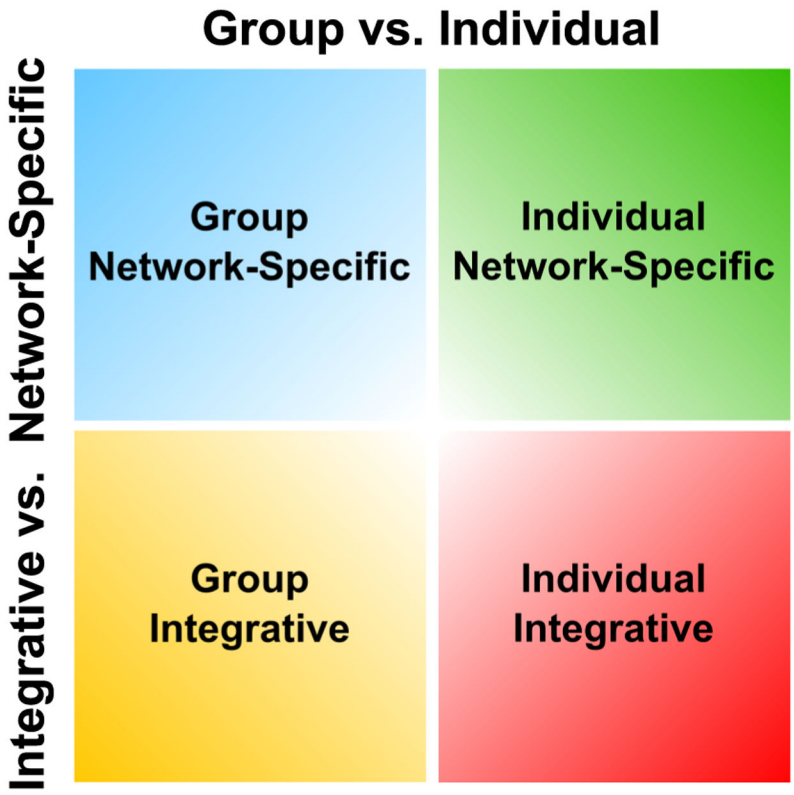

Figure 1. Framework for subcortical functional organization.

Subcortical RSFC was characterized along two principal axes, each with two levels (Group vs. Individual; Network specific vs. Integrative). “Group” refers to RSFC that is common across participants, whereas “Individual” refers to RSFC that is individually-specific. “Network specific” refers to regions of the subcortex with preferential RSFC to a single cortical network, whereas “Integrative” refers to regions of the subcortex with preferential RSFC to multiple cortical networks.

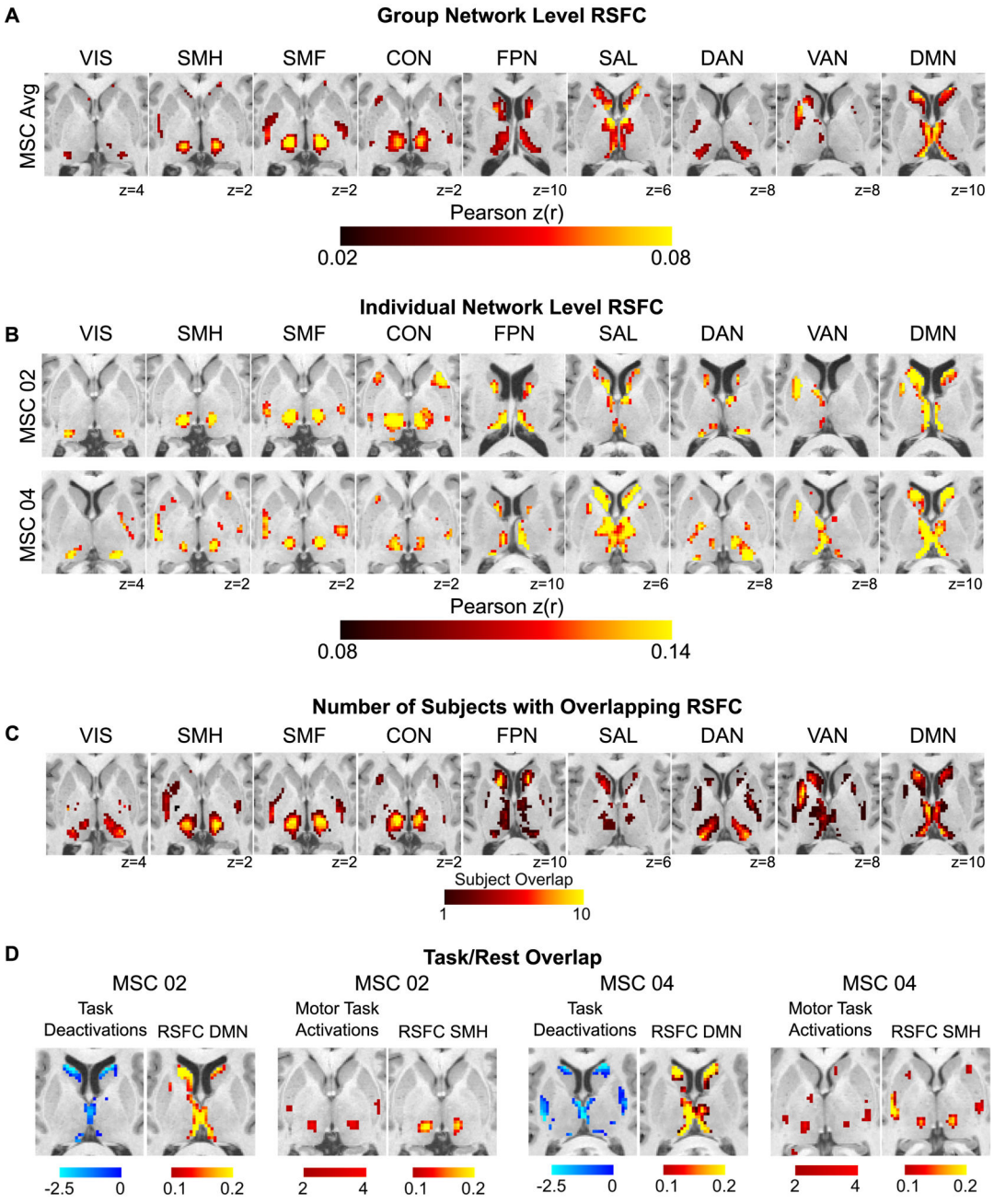

Figure 2. Subcortical RSFC is measurable at the individual level.

(A) Group-averaged subcortical RSFC for each cortical network. (B) Individual-level subcortical RSFC for each network from two representative MSC subjects, one male (MSC02) and one female (MSC04) (see Fig. S2 for all ten subjects). (C) Subject overlap showing the number of subjects with strong (top 10%) correlations with each network at that voxel. (D) Concordance between RSFC and task activations/deactivations within individuals. Task-evoked increases in BOLD activity during a motor task converge with peak RSFC in the somatomotor hand network. Task-evoked deactivations during a set of cognitive/ perceptual tasks converge with peak RSFC in the default-mode network. Anatomical left is

image left. VIS = visual; SMH = somatomotor hand; SMF = somatomotor face; CON = cingulo-opercular network; FPN = frontoparietal network; SAL = salience; DAN = dorsal attention network; VAN = ventral attention network; DMN = default-mode network.

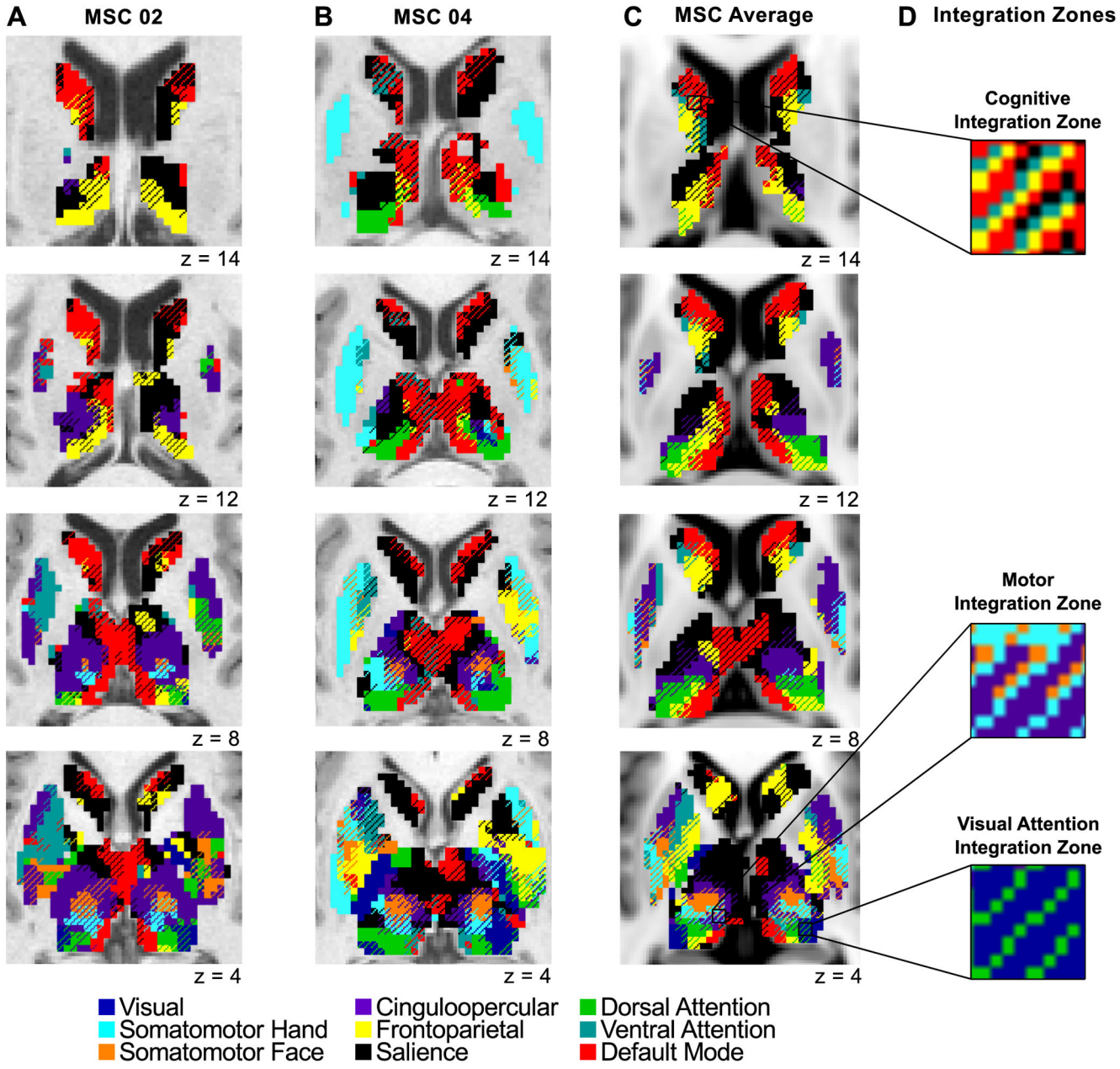

Figure 3. Network-specific and integrative functional zones in the basal ganglia and thalamus.

Data displayed for (A) one male representative subject (MSC02), (B) one female representative subject (MSC04), and (C) the group average (all subjects shown in Fig. S7). Voxels with preferential RSFC to one network (network-specific) are represented by solid colors, and voxels functionally connected to multiple networks (integrative) are represented by cross-hatching. Anatomical left is image left. (D) Zooming in on several integration zones; three distinct clusters of integration zones (see Fig. 5): cognitive integration zones, motor integration zones, and visual attention integration zones.

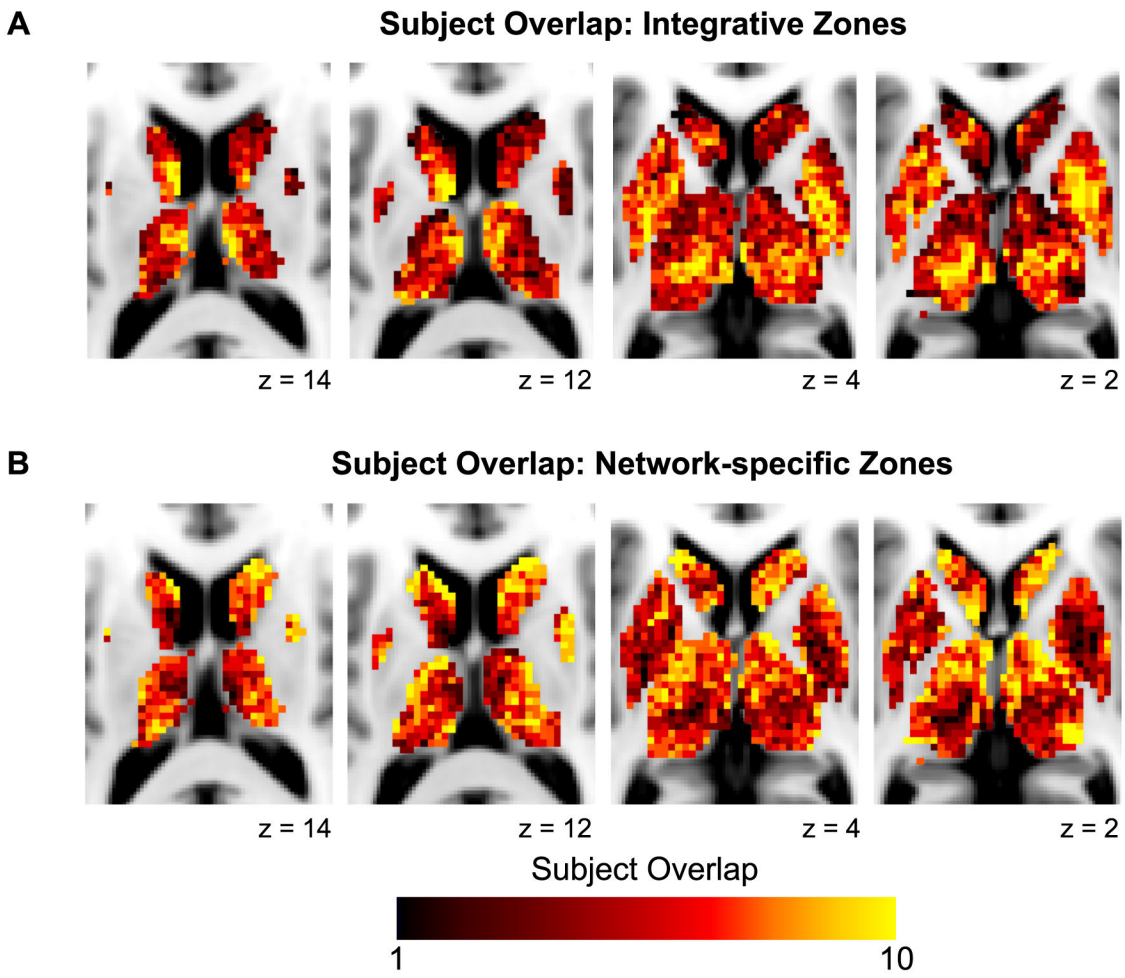

Figure 4. Overlap across individuals of integrative and network-specific functional zones.

Higher values represent voxels with (A) integrative functional zones present in multiple subjects and (B) network-specific functional zones present in multiple subjects.

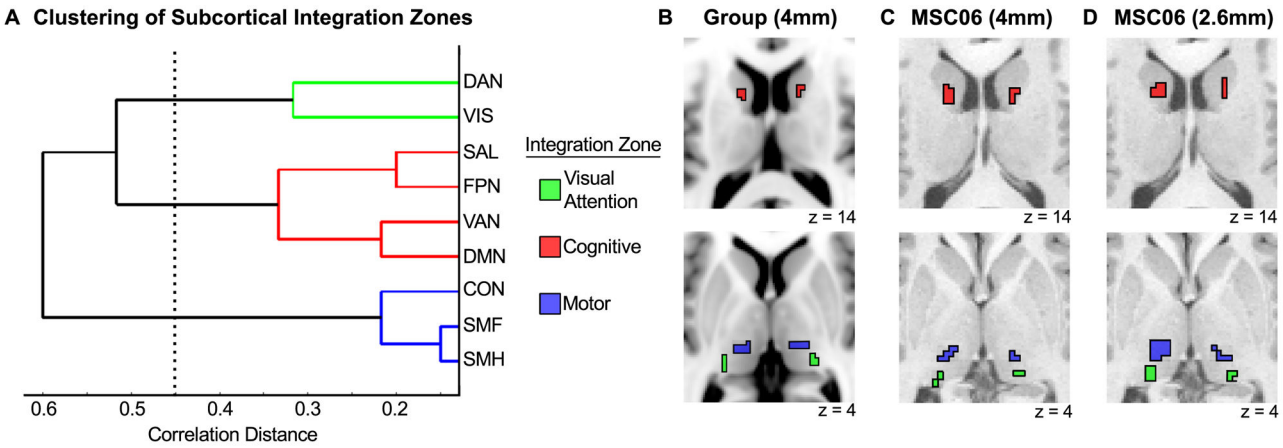

Figure 5. Three clusters of network integration are present in the subcortex.

(A) Hierarchical clustering revealed three clusters of network integration involving (1) dorsal attention and visual networks, (2) salience, frontoparietal, ventral attention, and default-mode networks, and (3) cingulo-opercular, somatomotor face, and somatomotor hand networks. (B) Most prominent locus of each cluster for the group average. (C) Most prominent locus of each cluster for an example individual (MSC06) with 4mm resolution data. (D) Most prominent locus of each cluster for the same individual (MSC06) with 2.6mm resolution data.

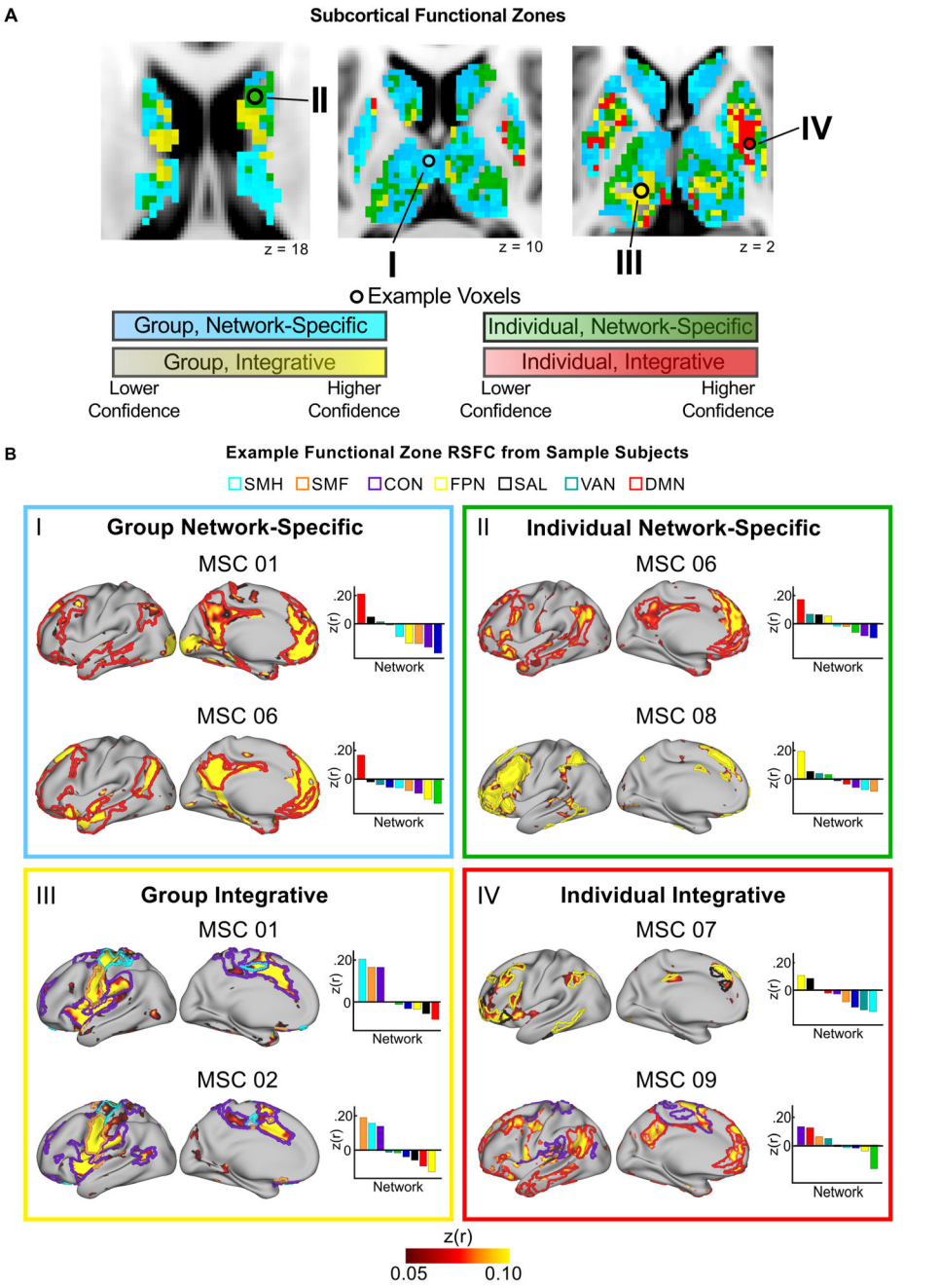

Figure 6. The subcortex contains four distinct functional zones: Group Network-Specific, Group Integrative, Individual Network-Specific, Individual Integrative.

(A) Anatomical distribution of each functional zone. Color gradation displays the confidence of zone assignment for each voxel as estimated by a jack-knifing procedure. (B) Typical examples of each type of functional zone using “example voxels” from panel A. Colored borders on the cortical surface represent the outline of the individual’s cortical networks that show strong RSFC with the example voxel. Bar graphs display RSFC correlations between the example voxel and each cortical network.

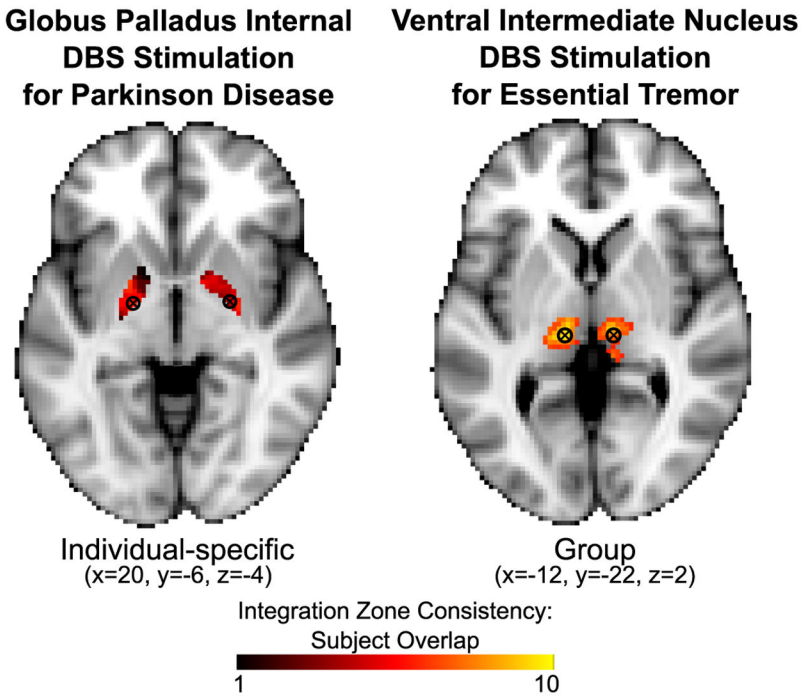

Figure 7. Overlap of integration zones and common sites of DBS.

Sites of DBS are shown with commonly targeted coordinates overlaid onto individual-specific (globus pallidus) and group (ventral intermediate thalamus) functional zones from the present study. Color gradation shows the consistency of the integration zones across subjects. The globus pallidus site, which has variable success rates, overlaps with an Individual Integrative zone. The ventral intermediate thalamus site, which has consistently high success rates, overlaps with a Group Integrative zone.

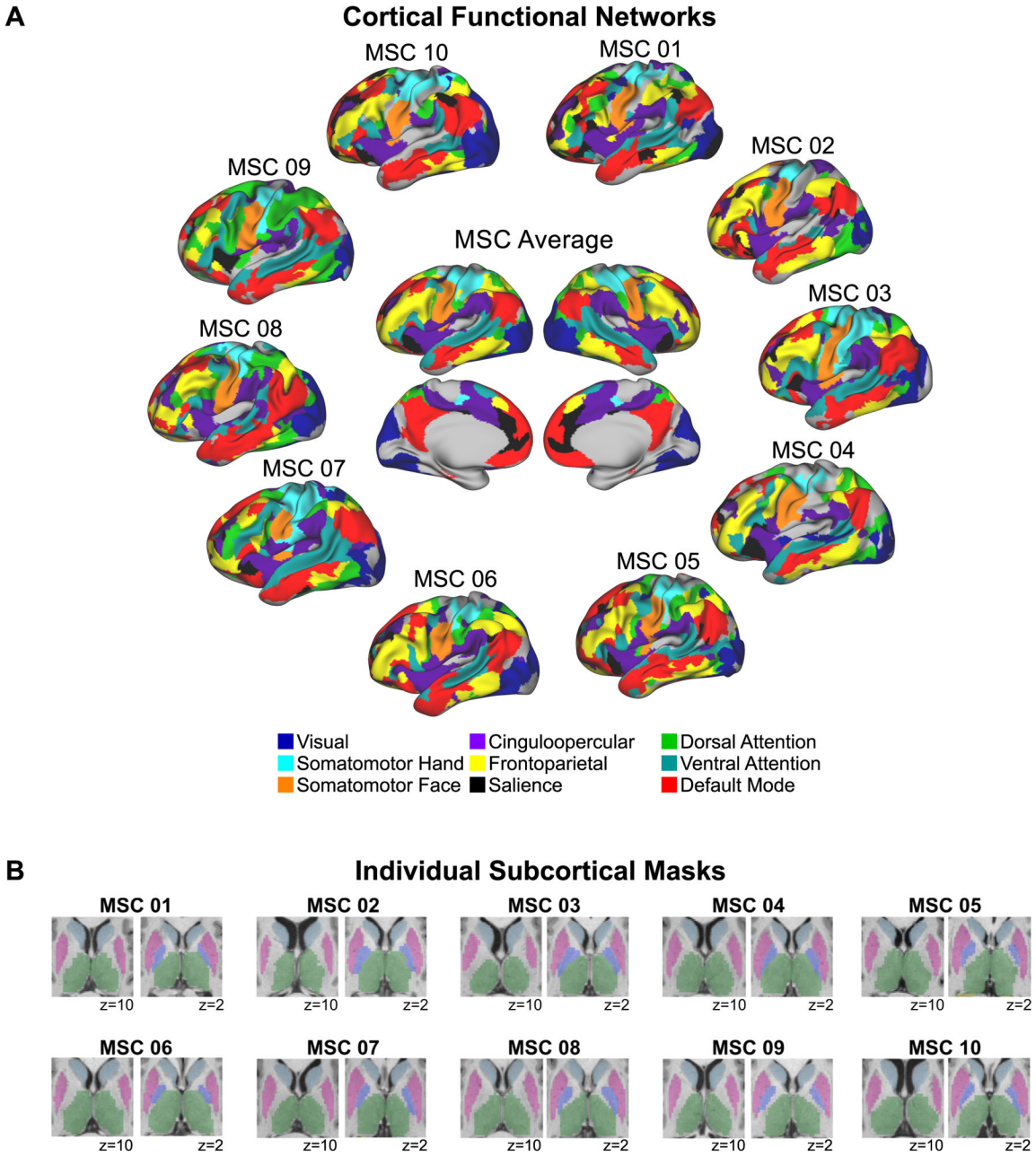

Figure 8. Functional cortical networks and subcortical voxels for each individual.

(A) Individually-defined functional networks (defined as in Gordon et al., 2017) and the group average functional networks are shown. Nine previously well-characterized functional networks were selected in order to investigate cortico-subcortical functional connectivity involving cortical networks that are described consistently using different methods and by multiple investigator groups (e.g., Damoiseaux et al., 2006; Gordon et al., 2016; Power et al., 2011; Yeo et al., 2011). Uncolored regions correspond to vertices that were not part of these nine networks according to the InfoMap network assignments. Note that including all 15 InfoMap networks (excluding unassigned and medial temporal vertices) did not change the results. (B) Subcortical masks from Freesurfer and manually edited using Freeview are

shown for each individual. Light blue = caudate; pink = putamen, violet = pallidum; green = thalamus.

Key Resources Table

REAGENT or RESOURCE	SOURCE	IDENTIFIER
Deposited Data		
Raw and processed MRI data	(Gordon et al., 2017b)	https://openfmri.org/dataset/ds000224 Accession # ds000224
Task fMRI activations	(Gordon et al., 2017b)	http://neurovault.org/collections/2447/
Psychological Image Collection at Stirling 2D face set		http://pics.psych.stir.ac.uk/
CNBC Tarrlab “Face Place” repository	(Righi et al., 2012)	wiki.cnbc.cmu.edu/Face_Place
Park Aging Mind Laboratory Face Database		agingmind.utdallas.edu/facedb
Libor Spacek’s Facial Imaging Database		cmp.felk.cvut.cz/~spacelib/faces/
English Lexicon Project	(Balota et al., 2007)	http://elexicon.wustl.edu/
Software and Algorithms		
Matlab	Mathworks	RRID:SCR_001622 https://www.mathworks.com/
Connectome Workbench	(Marcus et al., 2011)	RRID:SCR_008750 http://www.humanconnectome.org/software/connectome-workbench.html
Freesurfer	(Dale et al., 1999)	RRID:SCR_001847 https://surfer.nmr.mgh.harvard.edu/
FSL	(Smith et al., 2004)	RRID:SCR_002823 https://fsl.fmrib.ox.ac.uk/fsl/fslwiki
4dfp tools		ftp://imaging.wustl.edu/pub/raichlab/4dfp_tools/
Freesurfer to fs_LR pipeline	(Van Essen et al., 2012)	http://brainvis.wustl.edu
Parcellation code	(Gordon et al., 2016)	http://www.nil.wustl.edu/labs/petersen/Resources_files/Surface_parcellation_distribute.zip
Infomap	(Rosvall and Bergstrom, 2008)	www.mapequation.org